



Deposited via The University of Sheffield.

White Rose Research Online URL for this paper:

<https://eprints.whiterose.ac.uk/id/eprint/97067/>

Version: Accepted Version

---

**Article:**

Myers, R.J., Bernal, S.A. and Provis, J.L. (2014) A thermodynamic model for C-(N-)A-S-H gel: CNASH<sub>ss</sub>. Derivation and validation. *Cement and Concrete Research*, 66. pp. 27-47. ISSN: 0008-8846

<https://doi.org/10.1016/j.cemconres.2014.07.005>

---

Article available under the terms of the CC-BY-NC-ND licence  
(<https://creativecommons.org/licenses/by-nc-nd/4.0/>)

**Reuse**

This article is distributed under the terms of the Creative Commons Attribution-NonCommercial-NoDerivs (CC BY-NC-ND) licence. This licence only allows you to download this work and share it with others as long as you credit the authors, but you can't change the article in any way or use it commercially. More information and the full terms of the licence here: <https://creativecommons.org/licenses/>

**Takedown**

If you consider content in White Rose Research Online to be in breach of UK law, please notify us by emailing [eprints@whiterose.ac.uk](mailto:eprints@whiterose.ac.uk) including the URL of the record and the reason for the withdrawal request.

# A thermodynamic model for C-(N-)A-S-H gel:

## CNASH<sub>ss</sub>. Derivation and validation

Rupert J. Myers, Susan A. Bernal, John L. Provis \*

Department of Materials Science and Engineering, The University of Sheffield, Sir Robert  
Hadfield Building, Mappin St, Sheffield S1 3JD, UK

\* To whom correspondence should be addressed. Email [j.provis@sheffield.ac.uk](mailto:j.provis@sheffield.ac.uk), phone  
+44 114 222 5490, fax +44 114 222 5493

### Abstract

The main reaction product in Ca-rich alkali-activated cements and hybrid Portland cement (PC)-based materials is an calcium (alkali) aluminosilicate hydrate (C-(N-)A-S-H) gel. Thermodynamic models without explicit definitions of structurally-incorporated Al species have been used in numerous past studies to describe this gel, but offer limited ability to simulate the chemistry of blended PC materials and alkali-activated cements. Here, a thermodynamic model for C-(N-)A-S-H gel is derived and parameterised to describe solubility data for the CaO-(Na<sub>2</sub>O,Al<sub>2</sub>O<sub>3</sub>)-SiO<sub>2</sub>-H<sub>2</sub>O systems and alkali-activated slag (AAS) cements, and to chemical composition data for C-A-S-H gels. Simulated C-(N-)A-S-H gel densities and molar volumes are consistent with the corresponding values reported for AAS cements, meaning that the model can be used to describe chemical shrinkage in

24 these materials. Therefore, this model can provide insight into the chemistry of AAS cements at  
25 advanced ages, which is important for understanding the long-term durability of these materials.

26

27

## 28 **Keywords**

29

30 *B. Calcium-Silicate-Hydrate (C-S-H); B. Thermodynamic Calculations; D. Alkali Activated Cement; D.*

31 *Blended Cement; E. Modelling.*

32

33

## 34 **Nomenclature**

35

$a$	Extent of substitution of trivalent cation $R$ in bridging sites
$\dot{a}$	Ion size parameter in the extended Debye-Hückel equation (Å)
$a', b', \dots, e'$	Stoichiometric coefficients in the additivity method
$A_\gamma$	Temperature-dependent electrostatic parameter in the extended Debye-Hückel equation
$BCI$	Combined $BT$ , $CB$ and $IC$ sites ( $BCI = BT + CB + IC$ )
$b^{sc}$	Neutron scattering length (m)
$BT$	Bridging tetrahedra
$B_\gamma$	Pressure-dependent electrostatic parameter in the extended Debye-Hückel equation
$b_\gamma$	Short-range interaction parameter in the extended Debye-Hückel equation, $\text{kg}\cdot\text{mol}^{-1}$
$c$	Charge of the charge-balancing interlayer cation
$CB$	Interlayer charge-balancing species for bridging tetrahedra
$CL$	Chain length of an end-member in the sublattice solid solution model
$Cp^o$	Absolute isobaric heat capacity at standard state ( $\text{J}\cdot\text{mol}^{-1}\cdot\text{K}^{-1}$ )
$CU$	Interstitial 'solid solution' $\text{Ca}(\text{OH})_2$
$d_1, d_2$	Coefficients for the $CB$ sites
$e_1, e_2$	Coefficients for the $IC$ sites
$\Delta_f G^o$	Standard Gibbs free energy of formation ( $\text{J}\cdot\text{mol}^{-1}$ )
$G_m$	Gibbs free energy of mixing ( $\text{J}\cdot\text{mol}^{-1}$ )
$G_m^E$	Excess Gibbs free energy of mixing ( $\text{J}\cdot\text{mol}^{-1}$ )
$h$	The amount of water per dreierketten unit in a tobermorite-like structure
$\Delta_f H^o$	Standard enthalpy of formation ( $\text{J}\cdot\text{mol}^{-1}$ )

$i$	Species of the sublattice solid solution model
$I$	Ionic strength of the aqueous electrolyte phase in the extended Debye-Hückel equation, mol·kg <sup>-1</sup>
I, II, III, IV, V, VI	Stoichiometric coefficients of the sublattice sites in the solid solution model
$i_1i_2i_3\dots i_s$	End-member of the sublattice solid solution model written in terms of the species substituted in sublattice sites 1, 2, 3,..., $s$
$IC$	Interlayer charge-balancing species for the $TU$ sites
$IW$	Interlayer water
$k$	End-member of the sublattice solid solution model
$K_{so}$	Solubility product
$l$	Charge-balancing interlayer cation
$MW$	Molecular weight (g·mol <sup>-1</sup> )
$N_A$	Avogadro constant (6.022 x 10 <sup>23</sup> mol <sup>-1</sup> )
$n_s$	Sublattice sites
$R$	Trivalent cation in tetrahedral coordination
$R^*$	Universal gas constant (8.3145 J·mol <sup>-1</sup> ·K <sup>-1</sup> )
$s$	Index of sublattice site $n$
$S^o$	Absolute entropy at standard state (J·mol <sup>-1</sup> ·K <sup>-1</sup> )
$T$	Temperature (K)
$TU$	Main chain site, CaSiO <sub>3.5</sub> <sup>-</sup>
$u$	Interlayer H <sup>+</sup> content per dreierketten unit for the $TU$ sites
$U$	Term containing the Gibbs free energies for the reciprocal reactions (J·mol <sup>-1</sup> )
$V^o$	Standard molar volume (J·bar <sup>-1</sup> )
$x_{jw}$	Molar quantity of water in the extended Debye-Hückel equation, mol
$X_w$	Total molar amount of the aqueous phase in the extended Debye-Hückel equation, mol
$y_i^{ns}$	Site fraction of species $i$ in the sublattice site $n_s$
$z_j$	Charge of aqueous species $j$
$\alpha_k$	Activity of end-member $k$
$\gamma_j$	Activity coefficient of aqueous species $j$
$\Delta_{rcp}^oG$	Standard Gibbs free energy of a reciprocal reaction between end-members of the sublattice solid solution model
$\zeta$	Stoichiometric coefficient of the $s^{\text{th}}$ sublattice site
$\lambda_k$	Fictive activity coefficient of end-member $k$
$\mu$	Chemical potential (J·mol <sup>-1</sup> )
$\nu$	Fraction of bridging site vacancies per dreierketten unit
$\rho'$	Density of an end-member of the sublattice solid solution model (g·m <sup>-3</sup> )
$\rho^{sc}$	Neutron scattering length density (m <sup>-2</sup> )
$\Phi^o$	Standard thermodynamic property estimated by the additivity method
$\chi_k^{i,ns}$	Effective mole fraction of end-member $k$ containing species $i$ in sublattice site $n_s$

36

37

38

## 39        **1. Introduction**

40

41    A key factor governing the long-term performance of any cement or concrete is the stability of the  
42    reaction products constituting the solid binder. Work in this area has historically been targeted at  
43    understanding the chemistry of the primary reaction product in Portland cement (PC) materials,  
44    which is a Ca-rich ( $\text{Ca/Si} > 1.5$ ) calcium silicate hydrate (C-S-H)<sup>a</sup> gel [1]. A substantial amount of this  
45    research has been devoted to understanding the solubility of C-S-H gel [2-16], and development of  
46    thermodynamic models for this phase has been ongoing over the past decades [15, 17-22]. The Kulik  
47    and Kersten C-S-H thermodynamic model [17] has been applied extensively to successfully predict  
48    hydrated PC solid phase assemblages and pore solution compositions as a function of the bulk solid  
49    binder chemistry [23, 24]. The majority of published solubility data for C-S-H gel have been identified  
50    to fall onto several distinct solubility curves [8, 16], indicating that an important and complex  
51    structure-solubility relationship exists for this phase. More recently, a structurally-consistent C-S-H  
52    thermodynamic model has been developed [25], which has further improved the utility of the  
53    thermodynamic modelling approach in understanding the chemistry of PC materials.

54

55    Although the chemistry of hydrated neat PC materials is now relatively well established, many  
56    modern cements are comprised of blends of PC with Al-containing supplementary cementitious  
57    materials (SCMs), which react to form calcium aluminosilicate hydrate (C-A-S-H) gels with  
58    significantly lower Ca content ( $\text{Ca/Si} \leq 1.5$ ) [26, 27]. The level of Ca in the gel is reduced even further  
59    in alkali-activated slag (AAS) cements, which are formed through the reaction between ground  
60    granulated blast furnace slag (GBFS) and a highly alkaline solution (which are most often Na-based,  
61    although the products of activation with alternative alkalis such as K are generally similar [28]). The  
62    compositions of the C-A-S-H type gels formed in these cements (denoted C-(N)-A-S-H to reflect the

---

<sup>a</sup> Cement chemistry shorthand notation is used throughout the text: A,  $\text{Al}_2\text{O}_3$ ; C, CaO; S,  $\text{SiO}_2$ ; H,  $\text{H}_2\text{O}$ ; and N,  $\text{Na}_2\text{O}$ .

63 increased alkali content in addition to the high levels of Al incorporated into this phase) vary  
64 depending on the activation conditions, but are typically close to  $\text{Ca/Si} = 1$  [29].

65

66 Previous thermodynamic studies of PC/SCM blended cements [26, 30] and AAS cements [31] have  
67 utilised empirical descriptions of Al substitution in C-A-S-H and C-(N-)A-S-H gels (e.g. by attributing  
68 amounts of Al to these gels to match experimentally measured Al/Si values of the solid binders in  
69 the materials), or have neglected to account for the uptake of Al into these phases in the modelling  
70 performed, because existing C-S-H thermodynamic model formulations do not contain explicit  
71 definitions of Al [15, 17, 18, 21, 25]. The ability to formally account for the extent of Al incorporation  
72 into these models is important because it offers scope to significantly improve the level of detail and  
73 confidence in predictions of the solid phases formed in the  $\text{CaO-Al}_2\text{O}_3\text{-SiO}_2\text{-H}_2\text{O}$  system as simulated  
74 by thermodynamic modelling. Hence, the development of thermodynamic models with explicit  
75 descriptions of Al in C-A-S-H and C-(N-)A-S-H gels signifies an important advancement in how  
76 cementitious materials are modelled and understood.

77

78 Here, a thermodynamic model is proposed to account explicitly for the tetrahedral Al and Na species  
79 bound in C-(N-)A-S-H gel, and applied to simulate the chemistry of AAS cements as an initial  
80 example. This model may also be applicable to high-volume blended PC/SCM materials (e.g. CEM III  
81 blast furnace cements specified under the EN 197-1 standard) because the structurally-bound Al and  
82 alkali species are specified independently in the model formulation, and because the C-(N-)A-S-H  
83 and C-A-S-H gels formed in these materials and in AAS cements are similar in nanostructure and  
84 chemical composition [26].

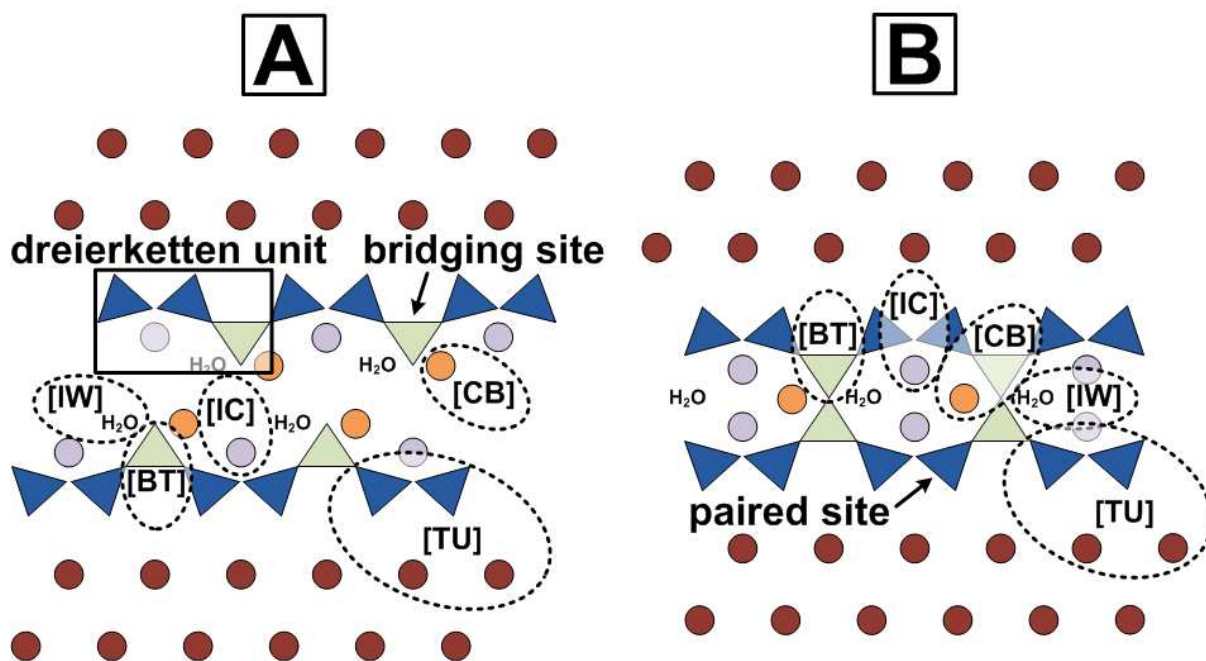
85

86

## 87 **2. The chemistry of AAS cements**

88

89 C-(N-)A-S-H gel, which is the dominant reaction product in AAS cements, contains aluminosilicate  
 90 chains arranged similarly to the disordered tobermorite-like phase C-S-H(I) [1], flanked on either side  
 91 by an 'interlayer' comprised of H<sub>2</sub>O and aqueous cations (e.g. Ca<sup>2+</sup>), and a Ca-O sheet (Figure 1).  
 92 These aluminosilicate chains are comprised of substituted 'dreierketten' units, which are repeating  
 93 sets of three silicate tetrahedra (Figure 1). C-(N-)A-S-H gel is believed to exclude Al-O-Al bonding  
 94 [32], and to only contain significant Al substitution in the bridging tetrahedral sites defined in Figure  
 95 1, not in the paired sites [33]. The mean chain length (MCL) is defined here as the number of silicate  
 96 and aluminate tetrahedra per C-(N-)A-S-H chain. MCL values for C-(N-)A-S-H gels in alkali-activated  
 97 slag binders with KOH or NaOH activating solutions have been calculated to be between 4 and 8 [34-  
 98 37] using a non-crosslinked tobermorite/calcium hydroxide representation of this phase [38],  
 99 compared with 6-11 for C-(N-)A-S-H gels derived from slag reacted with sodium silicate activators  
 100 [39].  
 101



102  
 103 **Figure 1.** Schematic representations of infinite chain length non-crosslinked (A) and crosslinked (B)  
 104 C-(N-)A-S-H gel structures, with sublattice sites labelled: *TU*; *BT*; *CB*; *IC*; *IW*, as defined in the text  
 105 (eqs.(2,4)). Light green and dark blue triangles are paired and bridging tetrahedral sites respectively,  
 106 dark red circles represent Ca sites in the Ca-O sheets, and the orange and purple circles are positively

107 charged species (typically  $\text{Ca}^{2+}$ ,  $\text{H}^+$ ,  $\text{Na}^+$  and/or  $\text{K}^+$ ) that charge-balance the aluminosilicate tetrahedra  
108 in the *BT* and *TU* sites respectively.  
109

110 Recent experimental results support a partially crosslinked structure for the C-(N-)A-S-H gel formed  
111 in  $\text{Na}_2\text{SiO}_3$ -activated slag binders:  $\text{Q}^3$  type species have been identified in deconvolutions of  $^{29}\text{Si}$   
112 magic angle spinning nuclear magnetic resonance (MAS NMR) spectra in silicate-activated slag  
113 cements [39, 40] and in laboratory-synthesised gels [41, 42]. A mixed crosslinked/non-crosslinked  
114 structural model was also needed to describe the mechanical properties of hydroxide and silicate-  
115 activated slag cements [36].  
116

117 The majority of AAS and related studies have used GBFS with  $\text{Al}_2\text{O}_3$  content  $\leq 14$  wt.% and NaOH,  
118 KOH or  $\text{Na}_2\text{O}\cdot m\text{SiO}_2\cdot x\text{H}_2\text{O}$  activators. Most studies using NaOH or KOH solutions have reported Mg-  
119 free binder compositions of  $0.7 \leq \text{Ca}/\text{Si} \leq 1.2$  and  $\text{Al}/\text{Si} \leq 0.25$  [35, 43-45], whereas those derived  
120 from  $\text{Na}_2\text{O}\cdot m\text{SiO}_2\cdot x\text{H}_2\text{O}$  solutions usually report Mg-free binder compositions of  $0.6 \leq \text{Ca}/\text{Si} \leq 1.2$ ,  
121  $\text{Al}/\text{Si} \leq 0.25$  [39, 40, 45, 46]. Laboratory-synthesised solids containing approximately phase-pure C-  
122 (N-)A-S-H gels have typically shown chemical compositions of  $0.5 < \text{Ca}/(\text{Al}+\text{Si}) \leq 1$  and  $\text{Al}/\text{Si} \leq 0.20$   
123 [42, 47, 48].  
124

125 Bound water is present in variable amounts in the interlayer spacing in C-S-H type structures, with  
126  $\text{H}_2\text{O}/\text{Si}$  ratios between 1.3-1.7 in gels with no adsorbed water [49], and must also be taken into  
127 account in development of thermodynamic models for C-(N-)A-S-H gels. The amount of structurally  
128 bound water in AAS cement is variable and not yet fully understood [50], so the water contents of  
129  $14\text{\AA}$  and  $11\text{\AA}$  tobermorites may also be used to guide the development of thermodynamic models  
130 for C-(N-)A-S-H gels. These minerals have bound  $\text{H}_2\text{O}/\text{Si}$  ratios of 1.17 and 0.83 respectively [51, 52].  
131  
132

### 133        **3. Sublattice solid solution model for C-(N-)A-S-H gel**

134

#### 135        **3.1 Sublattice solid solution definition**

136

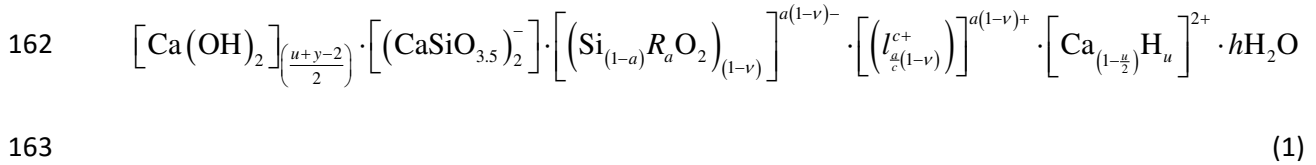
137        There exist several structural models that can describe C-S-H gels, as reviewed in detail by  
138        Richardson [53, 54]. However, only the ‘Substituted General Model’ (SGM) [38] and the ‘Crosslinked  
139        Substituted Tobermorite Model’ (CSTM) [39], can explicitly account for Al-substituted, alkali charge-  
140        balanced structures such as C-(N-)A-S-H gel using a fully flexible formulation of the gel chemistry.  
141        The CSTM describes C-(N-)A-S-H gel as a mixture of crosslinked and non-crosslinked tobermorite-like  
142        structures, and is therefore more generalised than the SGM for systems containing  $\text{Ca/Si} \leq 1.5$  (i.e.,  
143        excluding solid solution  $\text{Ca}(\text{OH})_2$ ). For  $\text{Ca/Si} \leq 1.5$  the treatments of non-crosslinked C-(N-)A-S-H gel  
144        components in the SGM and the CSTM are identical, with structural incorporation of Al and charge-  
145        balancing by positively-charged interlayer species such as  $\text{Na}^+$ . These structural models can be used  
146        to constrain thermodynamic models because they provide a structurally-consistent basis from which  
147        chemical compositions of C-(N-)A-S-H end-members can be determined.

148

149        Crosslinked and non-crosslinked C-(N-)A-S-H structures cannot always be distinguished from one  
150        another by bulk chemical composition alone, which complicates the ability to differentiate between  
151        these two structural types in thermodynamic models for this phase. Therefore, the SGM has been  
152        used as a basis from which to derive the chemical composition of the C-(N-)A-S-H gel here explicitly  
153        in terms of non-crosslinked structures, without precluding the possibility that the thermodynamic  
154        model may also implicitly represent the bulk chemistry of crosslinked C-(N-)A-S-H gels. It is also  
155        important to note that the C-S-H gel models derived by Kulik [25] used the ‘non-substituted general  
156        model’ developed by Richardson and Groves [55], which is a simpler model related to the SGM. The  
157        notation used by Kulik [25] and Richardson and Groves [38, 55] has been conserved where possible  
158        for clarity.

159

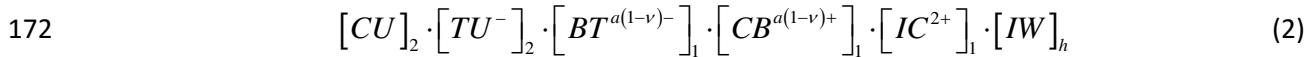
160 The SGM can be represented in terms of one dreierketten unit by eq.(1) (details of the derivation up  
161 to this point are provided in Appendix A):



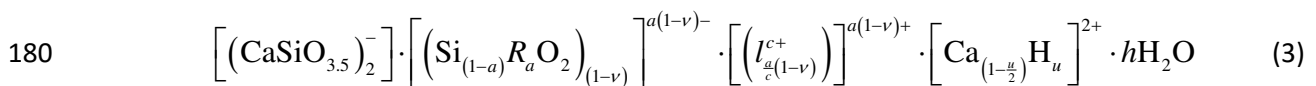
164 where  $R$  is a trivalent cation in tetrahedral coordination (e.g.  $\text{Al}^{3+}$ ),  $l$  is a charge-balancing interlayer  
165 cation (such as  $\text{Na}^+$ ,  $\text{Ca}^{2+}$  and/or  $\text{H}^+$ ) with a positive charge of  $c$ ,  $a$  is the extent of  $R$  substitution in  
166 bridging sites (Figure 1),  $\nu$  is the fraction of bridging site vacancies per dreierketten unit,  $u$  is the  
167 interlayer  $\text{H}^+$  content per dreierketten unit for the main chain sites ( $TU$ ,  $\text{CaSiO}_{3.5}^-$ ), and  $h$  defines the  
168 amount of water per dreierketten unit. The SGM explicitly defines Al substitution in bridging sites  
169 only, and excludes Al-O-Al bonding, consistent with Loewenstein's rule [32].

170

171 Eq.(1) can be equivalently written in sublattice notation as eq.(2):



173 where  $CU$  represents interstitial 'solid solution'  $\text{Ca}(\text{OH})_2$  [55],  $BT$  are the bridging tetrahedra ( $\text{Si}_{(1-}$   
174  $a)R_a\text{O}_{2(1-\nu)}^{a(1-\nu)-}$ ),  $CB$  are the interlayer charge-balancing species for the bridging tetrahedra ( $I_{a(1-\nu)/c}^{a(1-}$   
175  $\nu)+$ ),  $IC$  are the interlayer charge-balancing species for the  $TU$  sites ( $\text{Ca}_{(1-u/2)}\text{H}_u^{2+}$ ), and  $IW$  represents  
176 interlayer water ( $\text{H}_2\text{O}$ ). The  $CU$  sites in tobermorite are vacant (there is no interstitial 'solid solution'  
177  $\text{Ca}(\text{OH})_2$ ), and are therefore eliminated from the structural definition in eqs.(1-2). This limits the  
178 chemical composition of the sublattice solid solution model to  $0.67 \leq \text{Ca}/\text{Si} \leq 1.5$  and leads to eqs.(3-  
179 4):



181 
$$\left[ TU^- \right]_2 \cdot \left[ BT^{a(1-\nu)^-} \right]_1 \cdot \left[ CB^{a(1-\nu)^+} \right]_1 \cdot \left[ IC^{2+} \right]_1 \cdot \left[ IW \right]_h \quad (4)$$

182 This elimination of Ca(OH)<sub>2</sub> therefore provides the major limitation on the domain of applicability of  
 183 the model described here; it is not able to be used for Ca/Si ratios > 1.5, but is valuable for alkali-  
 184 activated cements and blended PC/SCM materials in which the composition of the C-(N-)A-S-H gel  
 185 formed falls below this ratio. The sublattice sites shown in eq.(4) are illustrated in Figure 1.

186

187 The *IC* sites are now modified to enable the *TU* sites to be charge-balanced by Na<sup>+</sup> species in  
 188 addition to the *BT* sites. The possible interlayer charge-balancing species in C-(N-)A-S-H gel are not  
 189 limited to Ca<sup>2+</sup>, H<sup>+</sup> and Na<sup>+</sup>, but these are the only species for which sufficient data have been  
 190 published to enable validation of the thermodynamic model developed here. Na-based solutions are  
 191 also the most relevant alkaline activators for commercial use because they are relatively inexpensive  
 192 and widely available [29]. The *BT* sites in C-(N-)A-S-H gel are mostly filled by vacancies, Si and/or Al  
 193 species, meaning that *R* = Al can also be specified. Eq.(3) is re-written with the modified *IC* sites and  
 194 with similarly modified *CB* sites, and with Al-substitution in the *BT* sites, which results in eq.(5):

195 
$$\left[ (CaSiO_{3.5})_2^- \right] \cdot \left[ (Si_{(1-a)}Al_aO_2)_{(1-\nu)} \right]^{a(1-\nu)^-} \cdot \left[ \left( Ca_{\left(\frac{1-d_1-d_2}{2}\right)} H_{d_1} Na_{d_2} \right)_{a(1-\nu)} \right]^{a(1-\nu)^+} \cdot \left[ Ca_{\left(\frac{2-e_1-e_2}{2}\right)} H_{e_1} Na_{e_2} \right]^{2+} \cdot hH_2O \quad (5)$$

196

197 where  $d_1 + d_2 \leq 1$  and  $e_1 + e_2 \leq 2$ .

198

199 While eqs.(4-5) are satisfactory for thermodynamic modelling, it is desirable to obtain a  
 200 thermodynamic model which is consistent with existing validated formulations such as the  
 201 downscaled CSH3T model [25]. In that model, the *BT*, *CB* and *IC* sites are combined into two  
 202 potentially-equivalent *BCI* sites that could have different substitutions via the choice of two  
 203 sublattice species, and the sublattice formula was 'downscaled' to 0.5 dreierketten units. The use of  
 204 two such sites, rather than a single *BCI* site, is beneficial because it increases the number of unique  
 205 chemical compositions that can be represented by the sublattice solid solution and can greatly

206 improve the fit of the thermodynamic model output to the validation data (e.g. solubility  
 207 measurements) for the same set of mixing rules used (e.g. simple random ideal mixing). However,  
 208 this means that end-member stoichiometries, and sublattice species and formulae are more likely to  
 209 be represented in terms of fractional quantities rather than integer amounts. Fractional expressions  
 210 obviously cannot directly correspond to atomistic-level structures, which means that  
 211 thermodynamic models developed in this way can only describe the chemistry of solid solutions on  
 212 the bulk scale rather than at the atomistic scale. Therefore, downscaling is useful in the  
 213 development of thermodynamic models to describe complex phases such as C-(N-)A-S-H gels with  
 214 atomistic structures that have not yet been fully resolved. Here, downscaling is essential to improve  
 215 the number of unique chemical compositions and the volume of experimental data described by the  
 216 sublattice solid solution model while keeping its formulation relatively simple, particularly because  
 217 this model is required to describe C-(N-)A-S-H gel chemistry in the complex AAS cement system. The  
 218 downscaled chemical and sublattice formulae (to 0.5 dreierketten units), written in terms of  
 219 potentially-equivalent *BCI* sites ( $BCI = BT + CB + IC$ ) and thus consistent with the downscaled  
 220 CSH3T model [25], are shown in eqs.(6-7) respectively:

$$221 \quad [CaSiO_{3.5}]^- \cdot \left[ \left\{ \left( Si_{(1-a)} Al_a O_2 \right)_{\frac{(1-\nu)}{2}} \cdot \left( Ca_{\left(\frac{1-d_1-d_2}{2}\right)} H_{d_1} Na_{d_2} \right)_{\frac{a(1-\nu)}{2}} \cdot \left( Ca_{\left(\frac{2-q-e_2}{2}\right)} H_{e_1} Na_{e_2} \right)_{\frac{1}{2}} \right\}^{\frac{0.5+}{2}} \right]_{\frac{1}{2}} \cdot \left[ \left( \frac{h}{2} \right) H_2O \right]_{\frac{1}{2}} \quad (6)$$

$$223 \quad [TU^-]_1 \cdot [BCI^{0.5+}]_1 \cdot [BCI^{0.5+}]_1 \cdot [IW]_{\frac{h}{2}} \quad (7)$$

224  
 225 Here, at least one additional (Al,Na)-containing sublattice species is necessary to represent C-(N-)A-  
 226 S-H gel chemistry, compared to previous thermodynamic models for the CaO-SiO<sub>2</sub>-H<sub>2</sub>O system.  
 227 Increasing the number of sublattice species and sites allows the description of a greater diversity of  
 228 bulk C-(N-)A-S-H gel chemical compositions, and facilitates independent incorporation of Na and Al  
 229 in C-S-H type structures. Additionally, as the quantities of bound water in C-(N-)A-S-H and C-S-H gels

230 are significantly different [50, 56], it is also necessary to allow for variation in the *IW* site. Here, C-(N-  
 231 )A-S-H gels are assumed to contain one mole of H<sub>2</sub>O in the *IW* site per 0.5 dreierketten units (*h* = 2),  
 232 because this is approximately equal to the chemistry of 11 Å and 14 Å tobermorites [51, 52] and the  
 233 C-A-S-H type gels formed in AAS binders (H<sub>2</sub>O/Si ≈ 1) [50].

234

235 These factors thus require the use of a sixth-order sublattice solid solution for the C-(N-)A-S-H  
 236 thermodynamic model developed here. This solid solution contains five *BCI* sites, with each carrying  
 237 a positive charge of 0.125 and grouped as shown in eqs.(8-9), and one variable *IW* site:

$$238 \left[ \text{CaSiO}_{3.5} \right]^- \cdot \left[ \text{H}_2\text{O} \right] \cdot \left[ \left( \text{Si}_{(1-a)}\text{Al}_a\text{O}_2 \right)_{\frac{(1-v)}{2}} \cdot \left( \text{Ca}_{\left(\frac{1-d_1-d_2}{2}\right)}\text{H}_{d_1}\text{Na}_{d_2} \right)_{\frac{a(1-v)}{2}} \cdot \left( \text{Ca}_{\left(\frac{2-e_1-e_2}{2}\right)}\text{H}_{e_1}\text{Na}_{e_2} \right)_{\frac{1}{2}} \right]_{\frac{1}{8}}^{0.125+} \cdot \left[ \left( \frac{h}{2} - 1 \right) \text{H}_2\text{O} \right]_{-8} \quad (8)$$

239

$$240 \left[ \text{TU}^- \right]_1 \cdot \left[ \text{IW}^* \right]_1 \cdot \left[ \text{BCI}^{0.125+} \right]_2 \cdot \left[ \text{BCI}^{0.125+} \right]_2 \cdot \left[ \text{BCI}^{0.125+} \right]_2 \cdot \left[ \text{BCI}^{0.125+} \right]_1 \cdot \left[ \text{BCI}^{0.125+} \right]_1 \cdot \left[ \text{IW} \right]_1 \quad (9)$$

241

242 where *IW*\* represents a fixed interlayer water site (with full occupancy of H<sub>2</sub>O but otherwise  
 243 identical to the *IW* site depicted in Figure 1). Eqs.(8-9) are the fundamental formulae that represent  
 244 the C-(N-)A-S-H thermodynamic model developed here.

245

### 246 3.2 End-member selection

247

248 As discussed in section 1, a goal of this study is to develop a sublattice solid solution model that can  
 249 describe the solubility and chemical composition of C-(N-)A-S-H gel in AAS cements. Based on the  
 250 sublattice solid solution definition established in eqs.(8-9), it is now necessary to select a set of end-  
 251 members, sublattice sites and species that can represent the chemistry of C-(N-)A-S-H gel.

252

253 Six species that can substitute into the five *BCI* sites given in eq.(9), and which are compatible with  
 254 the chemical formula for these sites (eq.(8)) and the chemistry of C-(N-)A-S-H gels in AAS cements,  
 255 were selected to represent a sublattice solid solution of the form shown in eq.(10):

$$256 \quad Q^* [A, B, C, D, E]_{\text{I}}^{n_1} [F, G, H, I, J]_{\text{II}}^{n_2} [K, L, M]_{\text{III}}^{n_3} [N, O, P, Q, R, S]_{\text{IV}}^{n_4} [T, U, V, W]_{\text{V}}^{n_5} [X, Y]_{\text{VI}}^{n_6} \quad (10)$$

257

258 Here, species *A, F, K, N, T* are  $\text{Ca}_{0.0625}\text{O}_{0.0625}\text{H}_{0.125}^{0.125+}$ , *B, G, L, O, U* are  $\text{Si}_{0.0625}\text{O}_{0.125}\text{H}_{0.125}^{0.125+}$  and  
 259 *D, I, M, Q, V* are  $\text{Si}_{0.0625}\text{O}_{0.125}\text{Na}_{0.125}^{0.125+}$ , which can be present in five different *BCI* sites, the species  
 260 *C, H, P* are  $\text{Al}_{0.0625}\text{O}_{0.125}\text{H}_{0.1875}^{0.125+}$  and *E, J, R* are  $\text{Al}_{0.0625}\text{Na}_{0.0625}\text{O}_{0.125}\text{H}_{0.125}^{0.125+}$ , which can fill four of  
 261 the *BCI* sites, the species *S, W* are  $\text{Ca}_{0.0625}\text{O}_{0.0625}\text{Na}_{0.125}^{0.125+}$ , which can fill two of the *BCI* sites, *X* is  
 262  $\text{H}_2\text{O}$ , *Y* is a vacancy ( $V_{IW}$ ), and  $Q^*$  is  $\text{CaSiO}_{3.5}^- \cdot \text{H}_2\text{O}$ . This combination of sublattice sites and species  
 263 was chosen as it comprises the least complex formulation of the sublattice solid solution that can  
 264 represent the chemistry of the C-(N-)A-S-H gel in AAS cements. In this work the coefficients  $\text{I}=2$ ,  
 265  $\text{II}=2$ ,  $\text{III}=2$ ,  $\text{IV}=1$ ,  $\text{V}=1$  and  $\text{VI}=1$  define the stoichiometry of the sublattice sites, and the  
 266 superscripts  $n_1, n_2, n_3, n_4, n_5$  and  $n_6$  correspond to the five *BCI* sites and single *IW* site in eq.(9).  
 267 Vacancies in *BCI* sites are included in the thermodynamic model via the  $\nu$  parameter in eq.(8).

268

269 A minimal set of eight end-members was chosen within this sublattice solid solution model to define  
 270 the C-(N-)A-S-H gel in this work, as shown in Table 1. This is the smallest number of end-members  
 271 that can resemble the chemistry of C-(N-)A-S-H gels (section 2) and describe the available solubility  
 272 data for AAS cement and the  $\text{CaO}-(\text{Na}_2\text{O}, \text{Al}_2\text{O}_3)\text{-SiO}_2\text{-H}_2\text{O}$  systems (section 6). The solid solution  
 273 contains three C-S-H end-members, one C-(N-)S-H end-member, two C-A-S-H end-members and two  
 274 C-(N-)A-S-H end-members. The C-S-H end-members have the same chemical compositions as the  
 275 T2C, T5C and TobH end-members of the downscaled CSH3T model (T2C\*, T5C\* and TobH\*  
 276 respectively) [25], which contain the *TU* site,  $h = 4$ , and two *BCI* sublattice species,  $\text{Si}_{0.25}\text{O}_{0.5}\text{H}_{0.5}^+$   
 277 and  $\text{Ca}_{0.25}\text{O}_{0.25}\text{H}_{0.5}^+$ , for  $a = 0$ , to cover the range  $0.67 \leq \text{Ca}/\text{Si} \leq 1.5$  in the  $\text{CaO-SiO}_2\text{-H}_2\text{O}$  system. One

This paper was published in *Cement and Concrete Research*, 66(2014):27-47. The version of record is available at <http://dx.doi.org/10.1016/j.cemconres.2014.07.005>

278 H<sub>2</sub>O molecule is also added per vacancy in the bridging tetrahedra for each of the eight end-  
279 members (determined by the value of  $\nu$ ).

280

281 **Table 1.** Chemical compositions of the eight end-members of the C-(N)-A-S-H thermodynamic model, and parameters chosen for use in eq.(8). One H<sub>2</sub>O  
 282 molecule is added to the *BCI* site per bridging site vacancy for consistency with the C-S-H thermodynamic model developed by Kulik [25].

End-member	$\nu$	$a$	$i_1$	$i_2$	$u_1$	$u_2$	$M$	Sublattice formula <sup>b</sup>	Chemical formula
5CA	0.5	1	1	0	1	0	2	$[(\text{CaSiO}_{3.5})^-]_1 \cdot [\text{H}_2\text{O}]_1 \cdot [\text{Al}_{0.0625}\text{O}_{0.125}\text{H}_{0.1875}^{0.125+}]_2 \cdot$ $[\text{Al}_{0.0625}\text{O}_{0.125}\text{H}_{0.1875}^{0.125+}]_2 \cdot [\text{Ca}_{0.0625}\text{O}_{0.0625}\text{H}_{0.125}^{0.125+}]_2 \cdot$ $[\text{Ca}_{0.0625}\text{O}_{0.0625}\text{H}_{0.125}^{0.125+}]_1 \cdot [\text{Ca}_{0.0625}\text{O}_{0.0625}\text{H}_{0.125}^{0.125+}]_1 \cdot [\text{V}_{\text{H}_2\text{O}}]_1$	$(\text{CaO})_{1.25}(\text{Al}_2\text{O}_3)_{0.125}(\text{SiO}_2)_1(\text{H}_2\text{O})_{1.625}$
INFCA	0	0.625	1	0	2	0	2	$[(\text{CaSiO}_{3.5})^-]_1 \cdot [\text{H}_2\text{O}]_1 \cdot [\text{Al}_{0.0625}\text{O}_{0.125}\text{H}_{0.1875}^{0.125+}]_2 \cdot$ $[\text{Al}_{0.0625}\text{O}_{0.125}\text{H}_{0.1875}^{0.125+}]_2 \cdot [\text{Si}_{0.0625}\text{O}_{0.125}\text{H}_{0.125}^{0.125+}]_2 \cdot$ $[\text{Al}_{0.0625}\text{O}_{0.125}\text{H}_{0.1875}^{0.125+}]_1 \cdot [\text{Si}_{0.0625}\text{O}_{0.125}\text{H}_{0.125}^{0.125+}]_1 \cdot [\text{V}_{\text{H}_2\text{O}}]_1$	$(\text{CaO})_1(\text{Al}_2\text{O}_3)_{0.15625}(\text{SiO}_2)_{1.1875}(\text{H}_2\text{O})_{1.65625}$
5CNA	0.5	1	0	1	0.5	0.5	2	$[(\text{CaSiO}_{3.5})^-]_1 \cdot [\text{H}_2\text{O}]_1 \cdot [\text{Al}_{0.0625}\text{Na}_{0.0625}\text{O}_{0.125}\text{H}_{0.125}^{0.125+}]_2 \cdot$ $[\text{Al}_{0.0625}\text{Na}_{0.0625}\text{O}_{0.125}\text{H}_{0.125}^{0.125+}]_2 \cdot [\text{Ca}_{0.0625}\text{O}_{0.0625}\text{H}_{0.125}^{0.125+}]_2 \cdot$ $[\text{Ca}_{0.0625}\text{O}_{0.0625}\text{Na}_{0.125}^{0.125+}]_1 \cdot [\text{Ca}_{0.0625}\text{O}_{0.0625}\text{Na}_{0.125}^{0.125+}]_1 \cdot [\text{V}_{\text{H}_2\text{O}}]_1$	$(\text{CaO})_{1.25}(\text{Na}_2\text{O})_{0.25}(\text{Al}_2\text{O}_3)_{0.125}(\text{SiO}_2)_1(\text{H}_2\text{O})_{1.375}$
INFCNA	0	0.625	0	1	1.25	0.75	2	$[(\text{CaSiO}_{3.5})^-]_1 \cdot [\text{H}_2\text{O}]_1 \cdot [\text{Al}_{0.0625}\text{Na}_{0.0625}\text{O}_{0.125}\text{H}_{0.125}^{0.125+}]_2 \cdot$ $[\text{Al}_{0.0625}\text{Na}_{0.0625}\text{O}_{0.125}\text{H}_{0.125}^{0.125+}]_2 \cdot [\text{Si}_{0.0625}\text{O}_{0.125}\text{Na}_{0.125}^{0.125+}]_2 \cdot$ $[\text{Al}_{0.0625}\text{Na}_{0.0625}\text{O}_{0.125}\text{H}_{0.125}^{0.125+}]_1 \cdot [\text{Si}_{0.0625}\text{O}_{0.125}\text{Na}_{0.125}^{0.125+}]_1 \cdot [\text{V}_{\text{H}_2\text{O}}]_1$	$(\text{CaO})_1(\text{Na}_2\text{O})_{0.34375}(\text{Al}_2\text{O}_3)_{0.15625}(\text{SiO}_2)_{1.1875}(\text{H}_2\text{O})_{1.3125}$
INFCN	0	0	1	0	0.75	1.25	2	$[(\text{CaSiO}_{3.5})^-]_1 \cdot [\text{H}_2\text{O}]_1 \cdot [\text{Si}_{0.0625}\text{O}_{0.125}\text{Na}_{0.125}^{0.125+}]_2 \cdot$ $[\text{Si}_{0.0625}\text{O}_{0.125}\text{Na}_{0.125}^{0.125+}]_2 \cdot [\text{Si}_{0.0625}\text{O}_{0.125}\text{H}_{0.125}^{0.125+}]_2 \cdot$ $[\text{Si}_{0.0625}\text{O}_{0.125}\text{Na}_{0.125}^{0.125+}]_1 \cdot [\text{Si}_{0.0625}\text{O}_{0.125}\text{H}_{0.125}^{0.125+}]_1 \cdot [\text{V}_{\text{H}_2\text{O}}]_1$	$(\text{CaO})_1(\text{Na}_2\text{O})_{0.3125}(\text{SiO}_2)_{1.5}(\text{H}_2\text{O})_{1.1875}$
T2C* <sup>a</sup>	1	0	0	0	0	0	4	$[(\text{CaSiO}_{3.5})^-]_1 \cdot [\text{H}_2\text{O}]_1 \cdot [\text{Ca}_{0.0625}\text{O}_{0.0625}\text{H}_{0.125}^{0.125+}]_2 \cdot$ $[\text{Ca}_{0.0625}\text{O}_{0.0625}\text{H}_{0.125}^{0.125+}]_2 \cdot [\text{Ca}_{0.0625}\text{O}_{0.0625}\text{H}_{0.125}^{0.125+}]_2 \cdot$ $[\text{Ca}_{0.0625}\text{O}_{0.0625}\text{H}_{0.125}^{0.125+}]_1 \cdot [\text{Ca}_{0.0625}\text{O}_{0.0625}\text{H}_{0.125}^{0.125+}]_1 \cdot [\text{H}_2\text{O}]_1$	$(\text{CaO})_{1.5}(\text{SiO}_2)_1(\text{H}_2\text{O})_{2.5}$
T5C* <sup>a</sup>	0.5	0	0	0	1	0	4	$[(\text{CaSiO}_{3.5})^-]_1 \cdot [\text{H}_2\text{O}]_1 \cdot [\text{Si}_{0.0625}\text{O}_{0.125}\text{H}_{0.125}^{0.125+}]_2 \cdot$ $[\text{Si}_{0.0625}\text{O}_{0.125}\text{H}_{0.125}^{0.125+}]_2 \cdot [\text{Ca}_{0.0625}\text{O}_{0.0625}\text{H}_{0.125}^{0.125+}]_2 \cdot$ $[\text{Ca}_{0.0625}\text{O}_{0.0625}\text{H}_{0.125}^{0.125+}]_1 \cdot [\text{Ca}_{0.0625}\text{O}_{0.0625}\text{H}_{0.125}^{0.125+}]_1 \cdot [\text{H}_2\text{O}]_1$	$(\text{CaO})_{1.25}(\text{SiO}_2)_{1.25}(\text{H}_2\text{O})_{2.5}$
TobH* <sup>a</sup>	0	0	0	0	2	0	4	$[(\text{CaSiO}_{3.5})^-]_1 \cdot [\text{H}_2\text{O}]_1 \cdot [\text{Si}_{0.0625}\text{O}_{0.125}\text{H}_{0.125}^{0.125+}]_2 \cdot$ $[\text{Si}_{0.0625}\text{O}_{0.125}\text{H}_{0.125}^{0.125+}]_2 \cdot [\text{Si}_{0.0625}\text{O}_{0.125}\text{H}_{0.125}^{0.125+}]_2 \cdot$ $[\text{Si}_{0.0625}\text{O}_{0.125}\text{H}_{0.125}^{0.125+}]_1 \cdot [\text{Si}_{0.0625}\text{O}_{0.125}\text{H}_{0.125}^{0.125+}]_1 \cdot [\text{H}_2\text{O}]_1$	$(\text{CaO})_1(\text{SiO}_2)_{1.5}(\text{H}_2\text{O})_{2.5}$

283 <sup>a</sup> The asterisks for the T2C\*, T5C\* and TobH\* end-members indicate that these components have the same bulk chemistry but slightly modified  
 284 thermodynamic properties relative to the T2C, T5C and TobH end-members of the downscaled CSH3T model [25].

285 <sup>b</sup> V<sub>H<sub>2</sub>O</sub> is a vacancy in the *IW* sublattice site.

286 As each species ( $A$  to  $Y$ ) is defined to only substitute into one site (i.e., species with the same  
 287 chemistry but occupying different sites are treated as being distinct), the site fraction of a species  $i$   
 288 in a given site  $n_s$ ,  $y_i^{n_s}$ , is defined as  $y_i^{n_s} = \sum (\chi_k^{i,n_s})$  for  $\sum (y_i^{n_s}) = 1$ . Here  $n_s \in \{n_1, n_2, n_3, n_4, n_5, n_6\}$   
 289 is the sublattice site,  $\chi_k^{i,n_s}$  is the effective mole fraction of end-member  $k$  containing the species  $i$  in  
 290 the sublattice site  $n_s$ , with  $\sum_k (\chi_k) = 1$ . In defining an end-member of the sublattice solid solution  
 291 model, the species present in the  $s^{th}$  sublattice site may be identified by the same subscript number  
 292 i.e.  $i_l$  is the species present in the sublattice site  $n_l$ , and  $i_l \in \{A, B, C, D, E\}$ . Thus an end-member  
 293 can be equivalently written in terms of its substituting species, i.e.  $k = i_1 i_2 i_3 \dots i_s$ .

294

295 The chain length ( $CL$ ) for each of the end-members, and the MCL of the C-(N)-A-S-H gel as a whole,  
 296 can then be calculated from eq.(11).

297 
$$CL = \frac{3}{\sum_k (\chi_k \nu_k)} - 1 \quad (11)$$

298

299 The fraction of bridging site vacancies per dreierketten unit,  $\nu$ , is shown in Table 1 for each end-  
 300 member of the C-(N)-A-S-H thermodynamic model. This equation represents the minimum chain  
 301 length possible for the end-members, and thus the minimum MCL of the C-(N)-A-S-H gel, because  
 302 eq.(11) implies that the end-members are strictly non-crosslinked. The chain lengths of crosslinked  
 303 C-(N)-A-S-H end-members would be calculated in the same way, but with a factor of two included  
 304 (i.e.  $CL_{crosslinked} = 2CL$ ) to reflect the double chain structures in these phases. Here, these crosslinked  
 305 and non-crosslinked structures were not explicitly differentiated in defining the end-members  
 306 (eqs.(8-9)), meaning that eq.(11) provides a lower bound on the MCLs of partially (or fully)  
 307 crosslinked C-(N)-A-S-H gels.

308

#### 4. Thermodynamic basis of the sublattice solid solution model

309

310

311 The chemical potential (partial molal Gibbs free energy),  $\mu_{i_1 i_2 i_3 \dots i_s}$ , of end-member  $i_1 i_2 i_3 \dots i_s$  in a multi-  
 312 component solid solution can be represented by eq.(12) [57]:

$$313 \quad \mu_{i_1 i_2 i_3 \dots i_s} = G_m + \left[ \frac{\partial G_m}{\partial y_{i_1}^{n_1}} + \frac{\partial G_m}{\partial y_{i_2}^{n_2}} + \frac{\partial G_m}{\partial y_{i_3}^{n_3}} + \dots + \frac{\partial G_m}{\partial y_{i_s}^{n_s}} \right] - \left[ \sum_i \left( y_i \frac{\partial G_m}{\partial y_i} \right) \right] \quad (12)$$

314 where  $G_m$  is the Gibbs free energy of mixing using the notation previously introduced, and can be  
 315 expressed by eq.(13) [58]:

$$316 \quad G_m = G^{mech} - TS_m^{id} + G_m^E \quad (13)$$

317 where  $G^{mech}$  is the Gibbs free energy of a compositionally-equivalent ‘mechanical mixture’ of simple  
 318 components to the solid solution phase,  $S_m^{id}$  is the difference in entropy between the ideal solid  
 319 solution for the solid phase and its end-member components (i.e. the configurational entropy), and  
 320  $G_m^E$  is the excess Gibbs free energy of mixing (representing the deviation of the solid solution from  
 321 ideality).

322

323 Here, the ‘compound energy formalism’ is used to define the surface of reference for the Gibbs free  
 324 energy of mixing as a weighted average of the Gibbs free energy of each of the (pure) end-members  
 325 in the C-(N-)A-S-H solid solution [57]. This is formally expressed by eq.(14) for a multi-site, multi-  
 326 component sublattice solid solution, assuming random mixing within each sublattice [59]:

$$327 \quad G_m = \left[ \sum_{n_1} \sum_{n_2} \sum_{n_3} \dots \sum_{n_s} \left( y_{i_1}^{n_1} y_{i_2}^{n_2} y_{i_3}^{n_3} \dots y_{i_s}^{n_s} \right) \cdot {}^o G_{i_1 i_2 i_3 \dots i_s} \right] +$$

$$328 \quad R^* T \left[ \text{I} \sum_{i_1} \left( y_{i_1} \ln y_{i_1} \right) + \text{II} \sum_{i_2} \left( y_{i_2} \ln y_{i_2} \right) + \text{III} \sum_{i_3} \left( y_{i_3} \ln y_{i_3} \right) + \dots + \zeta \sum_{i_s} \left( y_{i_s} \ln y_{i_s} \right) \right] + G_m^E \quad (14)$$

329 where  ${}^{\circ}G_{i_1i_2i_3\cdots i_s}$  is the standard Gibbs free energy of end-member  $i_1i_2i_3\cdots i_s$ ,  $R^*$  is the universal gas  
 330 constant,  $T$  is temperature and  $\zeta$  is the stoichiometric coefficient of the  $s^{\text{th}}$  sublattice site. The  
 331 random mixing assumption is appropriate here because it greatly simplifies the expression for the  
 332 configurational entropy and because the solid solution definition (eqs.(8-9)) does not represent  
 333 atomic-scale structures; assigning hypothetical weightings to non-physical mixing combinations  
 334 would not make physical sense. This choice is reasonable given that this is the first attempt to  
 335 develop a sublattice solid solution model for C-(N-)A-S-H gel, and will be validated in section 6  
 336 through the ability of the model to accurately describe chemical composition and solubility data for  
 337 this phase.

338

339 Eq.(14) can be expanded explicitly for the sublattice solid solution defined by the eight end-members  
 340 shown in Table 1. Substituting this expanded version of eq.(14) into eq.(12), defining a generalised  
 341 end-member with species  $A, F, K, N, T, X$  in sublattice sites  $n_1, n_2, n_3, n_4, n_5, n_6$  and then simplifying,  
 342 results in eq.(15):

$$343 \quad \mu_{AFKNTX} = {}^{\circ}G_{AFKNTX} + RT \left[ 2 \ln(y_A) + 2 \ln(y_F) + 2 \ln(y_K) + \ln(y_N) + \ln(y_T) + \ln(y_X) \right] + G_m^E + U \quad (15)$$

344

345 Equivalent relationships for  $\mu_{AFKNTX}$  can be written for all other combinations of sublattice site  
 346 occupancies. The  $U$  term contains the Gibbs free energies for the reciprocal reactions ( $\Delta_{rcp}{}^{\circ}G$ ), which  
 347 denotes the difference in Gibbs free energy between combinations of end-members in the sublattice  
 348 solid solution (which must by definition contain equal numbers of reactant and product terms). For  
 349 example, the reciprocal reaction (eq.(16)) has a corresponding Gibbs free energy of reaction given by  
 350 eq.(17):



$$352 \quad \Delta_{rcp}{}^{\circ}G_{LO} = {}^{\circ}G_{AFKOTX} + {}^{\circ}G_{AFLNTX} - {}^{\circ}G_{AFKNTX} - {}^{\circ}G_{AFLTOTX} \quad (17)$$

353

354 It is possible to make two key simplifications here. The first is setting  $G_m^E = 0$ , i.e. interactions  
355 between atoms in the same sublattice sites are neglected, meaning that the sublattice solid solution  
356 model is ideal. The second is that the Gibbs free energies of the reciprocal reactions in the solid  
357 solution are numerically approximated to zero ( $U = 0$ ). The reciprocal reaction terms describe the  
358 nearest-neighbour interactions in the solid solution, so are likely to influence end-member chemical  
359 potentials more than the next-nearest-neighbour interactions described by the excess Gibbs free  
360 energy terms. These terms are likely to be non-zero in C-(N-)A-S-H gels, because it is known that  
361 thermodynamic energetic differences arise from nearest-neighbour Si-Al substitution in  
362 aluminosilicate systems [60], but this approach can be validated by the good fit of the  
363 thermodynamic model to the published solubility and chemical composition data in the CaO-  
364 (Na<sub>2</sub>O,Al<sub>2</sub>O<sub>3</sub>)-SiO<sub>2</sub>-H<sub>2</sub>O systems (section 6). In defining the mixing rules in this way, the accuracy of  
365 the thermodynamic model is determined semi-empirically through the use of end-members with  
366 carefully selected chemical compositions and Gibbs free energies that internalise the nearest and  
367 next-nearest neighbour interactions in C-(N-)A-S-H gels, rather than through the explicit definition of  
368 these interactions. However, quantification of these interactions in terms of chemical potentials for  
369 hypothetical C-(N-)A-S-H end-members, and a better understanding of the solubility of C-(N-)A-S-H  
370 gels, will be important future steps in the model development.

371

372 Application of these assumptions to eq.(15) leads to the final, simplified formula for the chemical  
373 potential of an end-member in the C-(N-)A-S-H sublattice solid solution model (eq.(18)):

374 
$$\mu_{AFKNTX} = {}^oG_{AFKNTX} + RT \left[ 2 \ln(y_A) + 2 \ln(y_F) + 2 \ln(y_K) + \ln(y_N) + \ln(y_T) + \ln(y_X) \right] \quad (18)$$

375

376 The C-(N-)A-S-H thermodynamic model developed here is implemented in the GEM-Selektor v3  
377 thermodynamic modelling software (<http://gems.web.psi.ch/>) [61, 62]. Sublattice solid solution  
378 models can be specified in GEM-Selektor by modifying the activities of the chosen end-members

379 (Table 1) through the introduction of a ‘fictive activity coefficient’  $\lambda$ , which internalises the  
380 thermodynamic mixing relationships within the solid solution. This method was used in the C-S-H  
381 thermodynamic model developed by Kulik [25]. The fictive activity coefficient is defined by eq.(19):

$$382 \quad \lambda_k = \frac{\alpha_k}{\chi_k} \quad (19)$$

383 where  $\alpha_k$  is the activity of the  $k^{\text{th}}$  end-member, eq.(20):

$$384 \quad \mu_k = \mu_k^o + RT \ln(\alpha_k) \quad (20)$$

385

386 The fictive activity coefficient is defined by eliminating  $\mu_k$  and the  ${}^oG_{AFKNTX}$  term (equivalent to  $\mu_k^o$  as  
387 defined here) from eqs.(18,20), then substituting eq.(19) into the resulting equation and simplifying  
388 to obtain eq.(21):

$$389 \quad \ln(\lambda_{AFKNTX}) = \left[ 2 \ln(y_A) + 2 \ln(y_F) + 2 \ln(y_K) + \ln(y_N) + \ln(y_T) + \ln(y_X) \right] \\ - \ln(\chi_{AFKNTX}) \quad (21)$$

390 Relationships equivalent to eq.(21) can thus be obtained for all eight end-members (Table 1). The  
391 fictive activity coefficient relationships for these end-members are shown in Appendix B.

392

393

## 394 **5. Modelling method**

395

### 396 **5.1 Modelling system definition**

397 The kernel Nagra/PSI [63], which is the default thermodynamic database for GEM-Selektor v3  
398 (<http://gems.web.psi.ch/>) [61, 62], and the CEMDATA07 thermodynamic database [17, 23, 64-69],  
399 which contains data for various compounds commonly found in cement systems, were used during  
400 simulations. The ideal gas equation of state is used to describe the gases and the Truesdell-Jones  
401 form of the extended Debye-Hückel equation, eq.(22) [70], is used to describe the aqueous species.

402 
$$\log_{10} \gamma_j = \frac{-A_\gamma z_j^2 \sqrt{I}}{1 + a B_\gamma \sqrt{I}} + b_\gamma I + \log_{10} \frac{x_{jw}}{X_w} \quad (22)$$

403

404 Here,  $\gamma_j$  and  $z_j$  are the activity coefficient and charge of the  $j^{\text{th}}$  aqueous species respectively,  $A_\gamma$  and  $B_\gamma$   
405 are temperature and pressure-dependent electrostatic parameters,  $I$  is the ionic strength of the  
406 aqueous electrolyte phase,  $a$  is the ion size parameter,  $b_\gamma$  is a parameter that describes short-range  
407 interactions between charged aqueous species in an electrolyte solution (representing the  
408 predominant electrolyte in the system),  $x_{jw}$  is the molar quantity of water, and  $X_w$  is the total molar  
409 amount of the aqueous phase. Constant values of  $a$  (3.31 Å) and  $b_\gamma$  (0.098 kg/mol) are taken to  
410 represent the average ion size and common short-range interactions of charged aqueous species in a  
411 NaOH-dominated solution [70]. The water activity is calculated from the osmotic coefficient [70].

412

413 The extended Debye-Hückel equation is accurate at moderate ionic strengths (up to ~ 1 molal) [70],  
414 which is lower than the ionic strength in AAS pore solutions (~1-3 molal in sodium silicate activated  
415 slag cements, e.g. [71]), but this equation was chosen here as a first step in development of the  
416 thermodynamic model as it is directly encoded in GEM-Selektor. Additionally, the description of  
417 aqueous silicate speciation in the GEM-Selektor databases does not currently extend beyond dimeric  
418 silicate and aluminosilicate units, and adsorption of aqueous species onto simulated solid phases is  
419 also not fully taken into account. Use of an improved aqueous phase model, such as the Pitzer model  
420 [72] coupled with a more complete description of silicate oligomerisation [73], and description of  
421 sorption effects, are goals of future work.

422

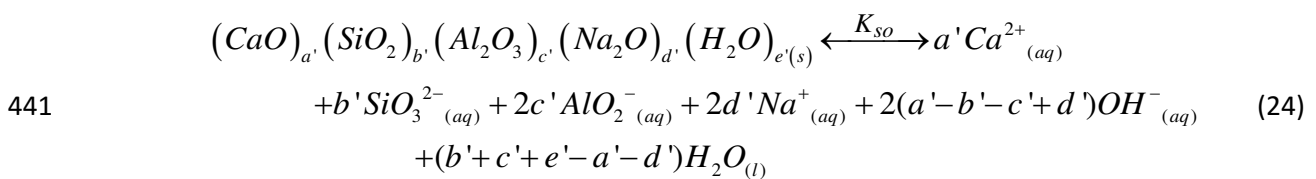
## 423 **5.2 Thermodynamic property estimation**

424 The standard absolute isobaric heat capacity ( $C_p^\circ$ ) and absolute entropy at standard state ( $S^\circ$ ) of the  
425 five (Al,Na)-containing C-(N-)A-S-H end-members were estimated using the additivity method and  
426 eq.(23), defined in terms of structurally-relevant constituents: T2C (the Ca-rich end-member of the

427 downscaled CSH3T model [25],  $(CaO)_{1.5}(SiO_2)_1(H_2O)_{2.5}$ , portlandite  $(Ca(OH)_2)$ , amorphous  $SiO_2$ ,  
 428 gibbsite  $(Al(OH)_3)$  and  $NaOH_{(s)}$ .

$$\begin{aligned} \Phi^o_{(CaO)_a'(SiO_2)_b'(Al_2O_3)_c'(Na_2O)_d'(H_2O)_e'} &= \frac{1}{2}(5a' - 3e' + 9c' + 3d')\Phi^o_{Ca(OH)_2} \\ &+ (b' - e' + a' + 3c' + d')\Phi^o_{SiO_2} + 2c'\Phi^o_{Al(OH)_3} + 2d'\Phi^o_{NaOH} \\ &+ (e' - a' - 3c' - d')\Phi^o_{(CaO)_{1.5}(SiO_2)_1(H_2O)_{2.5}} \end{aligned} \quad (23)$$

430  
 431 Here  $\Phi^o$  denotes the standard thermodynamic property undergoing estimation ( $Cp^o$  or  $S^o$ ),  $a'$ ,  $b'$ ,  $c'$ ,  
 432  $d'$ ,  $e'$  are the stoichiometric coefficients for the respective oxide components  $CaO$ ,  $SiO_2$ ,  $Al_2O_3$ ,  
 433  $Na_2O$  and  $H_2O$ , and the numerical coefficients for these terms are the values that result from solving  
 434 the elemental balance for eq.(23). The thermodynamic properties of the constituent phases are  
 435 provided in Appendix C, and are consistent with the Nagra/PSI [63] and CEMDATA07 thermodynamic  
 436 databases [17, 23, 64-69]. The additivity method is expected to yield relatively small errors in  
 437 estimated values for  $Cp^o$  and  $S^o$  if suitable constituents are chosen [74]. The changes in  $S^o$  and  $Cp^o$ ,  
 438 and the solubility product ( $K_{so}$ ) of the (Al,Na)-containing C-(N)-A-S-H end-members for the  
 439 dissociation reaction represented by eq.(24), were determined to enable thermodynamic property  
 440 calculations in GEM-Selektor:



442  
 443 The ReacDC module in GEM-Selektor was used to determine the standard partial molal Gibbs free  
 444 energies ( $\Delta_f G^o$ ) and enthalpies of formation ( $\Delta_f H^o$ ) for the proposed C-(N)-A-S-H end-members by  
 445 specifying 'optimised' solubility products for the reaction shown in eq.(24), the value of  $S^o$   
 446 determined via the additivity method (using the components listed previously), and the change in  $S^o$   
 447 of the dissociation reaction (eq.(24)). The Gibbs free energies (and thus the enthalpies) of the T2C\*,

448 T5C\* and TobH\* end-members were modified slightly from the values reported in the downscaled  
 449 CSH3T model [25], and solubility products of the (Al,Na)-containing C-(N-)A-S-H end-members were  
 450 selected, to obtain the optimised fit of the thermodynamic model to the solubility and solid phase  
 451 chemistry data in the CaO-(Na<sub>2</sub>O,Al<sub>2</sub>O<sub>3</sub>)-SiO<sub>2</sub>-H<sub>2</sub>O [2-15, 41, 42, 48, 75-81] and AAS cement systems  
 452 [71, 82-84] used in model validation (section 6). All other thermodynamic parameters of the T2C\*,  
 453 T5C\* and TobH\* end-members were adopted directly from the downscaled CSH3T model.  
 454  
 455 Standard molar volumes ( $V^{\circ}$ ) of the (Al,Na)-containing C-(N-)A-S-H end-members were determined  
 456 from density calculations using the method proposed by Thomas et al. [50], but extended to include  
 457 Na species via eq.(25):

$$458 \quad \rho^{sc}_{CNASH} = N_A \rho'_{CNASH} \left[ \frac{\left(\frac{CaO}{SiO_2}\right) b^{sc}_{CaO} + b^{sc}_{SiO_2} + \left(\frac{Al_2O_3}{SiO_2}\right) b^{sc}_{Al_2O_3} + \left(\frac{Na_2O}{SiO_2}\right) b^{sc}_{Na_2O} + \left(\frac{H_2O}{SiO_2}\right) b^{sc}_{H_2O}}{MW_{CNASH}} \right] \quad (25)$$

459 where the  $b^{sc}$  parameters are the established neutron scattering lengths for CaO, SiO<sub>2</sub>, Al<sub>2</sub>O<sub>3</sub>, Na<sub>2</sub>O  
 460 and H<sub>2</sub>O,  $\rho^{sc}$  is the scattering length density taken from the literature [50],  $\rho'_{CNASH}$  is the predicted  
 461 density of a C-(N-)A-S-H end-member,  $N_A$  is Avogadro's number,  $MW_{CNASH}$  is the molecular weight of  
 462 a C-(N-)A-S-H end-member, and the ratios CaO/SiO<sub>2</sub>, Al<sub>2</sub>O<sub>3</sub>/SiO<sub>2</sub>, Na<sub>2</sub>O/SiO<sub>2</sub>, and H<sub>2</sub>O/SiO<sub>2</sub> are molar  
 463 composition ratios of a C-(N-)A-S-H end-member. The optimised thermodynamic properties for the  
 464 C-(N-)A-S-H end-members are summarised in Table 2.

465

466 **Table 2.** Thermodynamic properties, densities and the change in thermodynamic properties for the  
 467 dissociation reaction (eq.(24)) for the end-members of the C-(N-)A-S-H solid solution (25°C, 1 bar)

Standard thermodynamic properties and density						
End-member	$V^{\circ}$ (cm <sup>3</sup> /mol)	$\Delta_f H^{\circ}$ (kJ/mol)	$\Delta_f G^{\circ}$ (kJ/mol)	$S^{\circ}$ (J/mol.K)	$C_p^{\circ}$ (J/mol.K)	$\rho'_{CNASH}$ (g/cm <sup>3</sup> )
5CA	57.3	-2491	-2293	163	177	3.01
INFCA	59.3	-2551	-2343	154	181	2.92
5CNA	64.5	-2569	-2382	195	176	2.84
INFCNA	69.3	-2667	-2474	198	180	2.72
INFCN	71.1	-2642	-2452	186	184	2.63
T2C* <sup>a</sup>	80.6	-2721	-2465	167	237	2.35
T5C* <sup>a</sup>	79.3	-2780	-2517	160	234	2.40

TobH* <sup>a</sup>	85.0	-2831	-2560	153	231	2.25
Change in thermodynamic properties for the dissociation reaction (eq.(24))						
End-member	$\Delta_r V^\circ$ (cm <sup>3</sup> /mol)	$\Delta_r H^\circ$ (kJ/mol)	$\Delta_r G^\circ$ (kJ/mol)	$\Delta_r S^\circ$ (J/mol.K)	$\Delta_r Cp^\circ$ (J/mol.K)	$\log_{10}(K_{so})$
5CA	-17.9	-4.0	61.4	-219	-29.3	-10.75
INFCA	5.1	0.58	50.8	-168	160	-8.90
5CNA	-37.1	-18.8	59.4	-262	-115	-10.4
INFCNA	-21.3	-10.8	57.1	-228	41.5	-10.0
INFCN	-12.5	-6.2	61.1	-226	144	-10.7

468 <sup>a</sup> The  $\log_{10}(K_{so})$  values for the T2C\*, T5C\* and TobH\* end-members, for the dissociation reaction  
469 eq.(24), are -11.6, -10.5 and -7.9 respectively.

470

471

## 472 6. Application of the thermodynamic model in GEM-Selektor

473

### 474 6.1 Approach

475 The success of a thermodynamic model is measured in terms of its ability to describe the available  
476 thermochemical data in the target system(s) - here, for Ca-rich alkali-activated cements such as AAS  
477 cements and hybrid alkali-activated/PC materials - and its ability to predict the chemistry of  
478 simulated systems where experimental data are either not available or are difficult to obtain. Hence,  
479 thermodynamic models for cements must be developed using existing experimental results such as  
480 solubility measurements [8, 47], solid product assemblages [35, 37, 43], and/or the chemistry of C-  
481 (N-)A-S-H gels [42]. An extensive set of experimental solubility data in the CaO-SiO<sub>2</sub>-H<sub>2</sub>O system is  
482 available for the development of thermodynamic models for C-S-H gels [2-15], but the use of such  
483 information to develop models for C-(N-)A-S-H gels is significantly more complicated. Solubility  
484 measurements in the CaO-Na<sub>2</sub>O-Al<sub>2</sub>O<sub>3</sub>-SiO<sub>2</sub>-H<sub>2</sub>O system are not available in sufficient detail to enable  
485 development of thermodynamic models using this information alone, meaning that validation  
486 against other data is necessary. In this light, AAS cements provide an opportunity to validate the  
487 thermodynamic model; these materials are described mostly in terms of the more complex CaO-  
488 Na<sub>2</sub>O-Al<sub>2</sub>O<sub>3</sub>-SiO<sub>2</sub>-H<sub>2</sub>O-MgO system, but are relatively well characterised. Hence, the thermodynamic

489 model here is validated for the less complex  $\text{CaO}-(\text{Na}_2\text{O},\text{Al}_2\text{O}_3)\text{-SiO}_2\text{-H}_2\text{O}$  systems, and also AAS  
490 cements. The ability of the thermodynamic model to predict solid phase assemblages in these  
491 systems will be discussed in a subsequent publication.

492

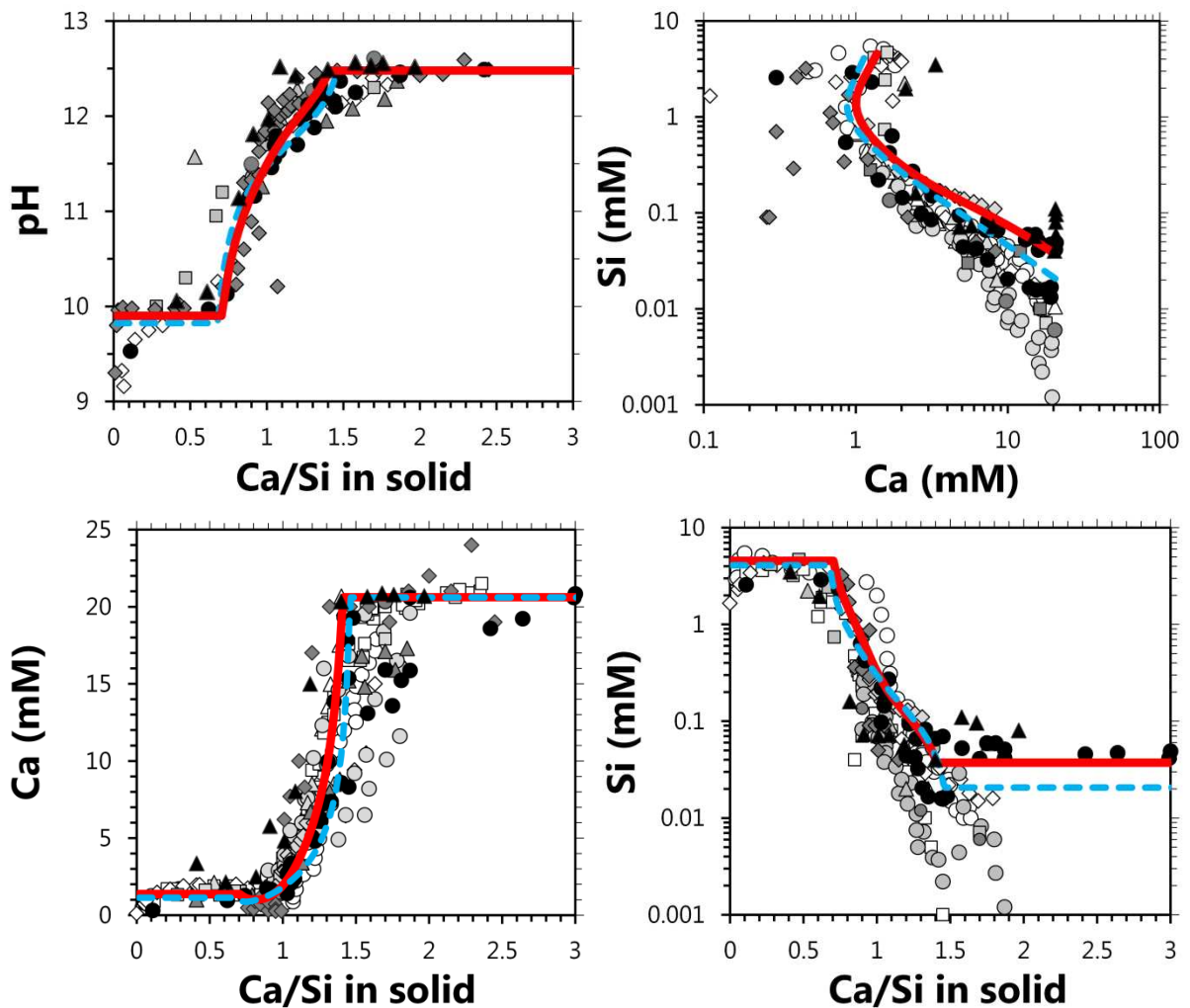
493 GEM-Selektor simulations for the  $\text{CaO-SiO}_2\text{-H}_2\text{O}$  and  $\text{CaO}-(\text{Na}_2\text{O},\text{Al}_2\text{O}_3)\text{-SiO}_2\text{-H}_2\text{O}$  systems were  
494 performed at a constant temperature and pressure of 25°C and 1 bar, using 1 g of each of the gases  
495  $\text{O}_2(\text{g})$  and  $\text{N}_2(\text{g})$ . Simulations were performed by adding  $\text{H}_2\text{O}$ ,  $\text{NaOH}$ ,  $\text{CaO}$ ,  $\text{Al}(\text{OH})_3$  and  $\text{SiO}_2$  at a fixed  
496 liquid/solid ratio = 50 using a basis of 1000 g  $\text{H}_2\text{O}$ . The C-(N-)A-S-H thermodynamic model developed  
497 here (CNASH\_ss) was used in all simulations. This model is provided as Electronic Supplementary  
498 Information, in the correct format for use in GEM-Selektor v3. The data used for the other gases,  
499 aqueous species and solid phases included in the simulations, in addition to the C-(N-)A-S-H  
500 thermodynamic model developed here, are shown in Appendix C.

501

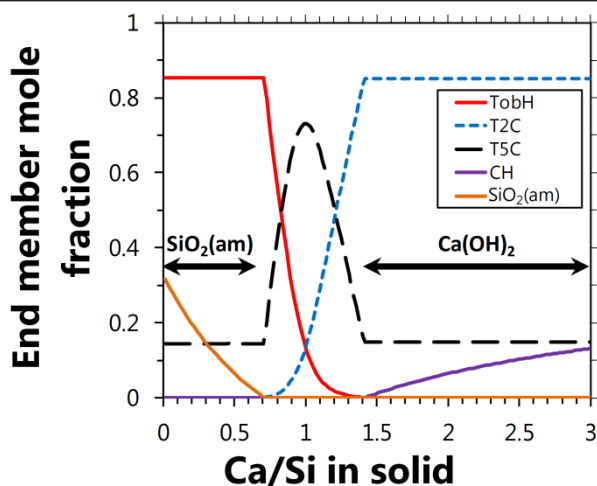
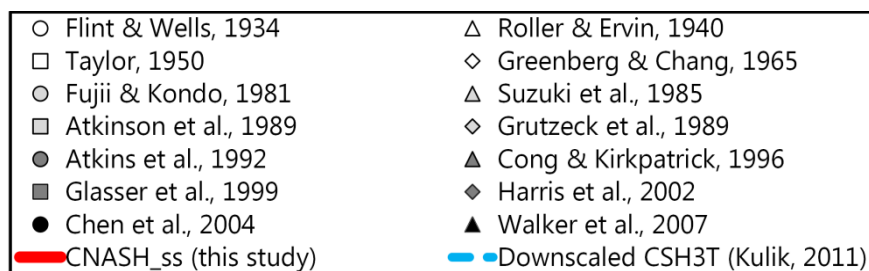
## 502 **6.2 Model validation in the $\text{CaO-SiO}_2\text{-H}_2\text{O}$ system**

503 An extensive body of solubility data for the  $\text{CaO-SiO}_2\text{-H}_2\text{O}$  system is available [2-15], which has been  
504 used to develop thermodynamic models for C-S-H gels in the past [15, 17, 18, 22, 25]. The fit of the  
505 new model to these data (Figure 2) is very good regarding description of the available data for pH,  
506 for concentrations of  $[\text{Ca}] < 2 \text{ mmol/L (mM)}$  and  $[\text{Si}] > 0.1 \text{ mM}$ , and for Ca and Si solubilities up to a  
507 molar Ca/Si ratio in the solid  $\approx 1.3$ . The thermodynamic model is less consistent with the full body of  
508 available data at higher dissolved Ca concentrations, lower aqueous Si concentrations, and higher  
509 Ca/Si ratios in the solid, but matches more closely with the more recently published data,  
510 particularly the measurements reported in [8]. The poorer fit of the thermodynamic model to these  
511 data indicate that it is partly limited by the assumption of no additional solid solution  $\text{Ca}(\text{OH})_2$ ; the  
512 simulated C-S-H gels are in equilibrium with portlandite for  $\text{Ca/Si} > 1.4$  and amorphous  $\text{SiO}_2$  is  
513 simulated at  $\text{Ca/Si}$  ratios in the solid  $\leq 0.67$  (Figure 2). It has previously been proposed [8] that C-S-H  
514 solubility varies as a function of the nanostructure of this phase, which is much more pronounced for

515 Ca/Si > 1 when many nanostructural configurations and potential bonding environments for Ca are  
516 possible (for example, Ca can be accommodated in the *CB* and *IC* sites here). This would mean that  
517 C-S-H thermodynamic models with a single curve for the solubility-structure relationships in these  
518 gels are inherently unable to describe the full range of available solubility data for this phase.  
519 However, the compositional region that is described accurately by the thermodynamic model is the  
520 region of principal importance for cementitious materials with compositions in the CaO-Na<sub>2</sub>O-Al<sub>2</sub>O<sub>3</sub>-  
521 SiO<sub>2</sub>-H<sub>2</sub>O system, which typically contain C-(N-)A-S-H gels with Ca/Si ≤ 1.2 (as discussed in section 2).  
522



525



526

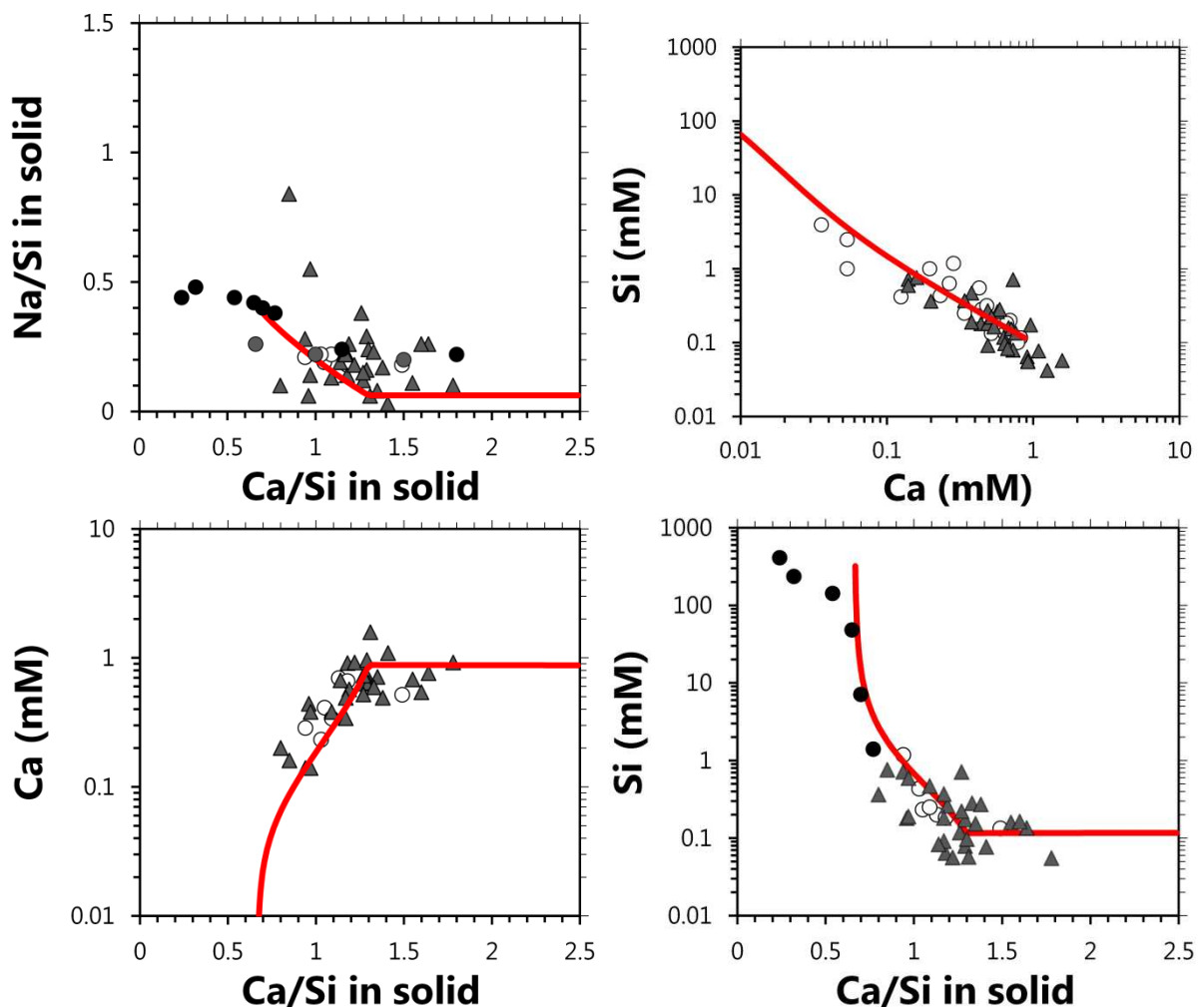
527 **Figure 2.** Comparison of the simulation results (25°C, 1 bar, water/solids mass ratio = 50) using the  
 528 thermodynamic model developed here (CNASH\_ss, bold red traces) to the downscaled CSH3T model  
 529 (dashed blue traces) [25] and published solubility data in the CaO-SiO<sub>2</sub>-H<sub>2</sub>O system [2-15]. Additional  
 530 plots are provided in Appendix D for the MCL and bulk chemistry results. The thermodynamic  
 531 properties of the phases included in these simulations are given in Appendix C.  
 532

### 533 6.3 Model validation in the CaO-Na<sub>2</sub>O-SiO<sub>2</sub>-H<sub>2</sub>O system

534 Significantly fewer thermochemical data are available for cements in the more complex CaO-Na<sub>2</sub>O-  
 535 SiO<sub>2</sub>-H<sub>2</sub>O system than in the CaO-SiO<sub>2</sub>-H<sub>2</sub>O system. Simulations for the CaO-Na<sub>2</sub>O-SiO<sub>2</sub>-H<sub>2</sub>O system  
 536 (Figure 3) were performed at bulk NaOH concentrations of 0.25, 0.5, 1 and 3 mol/L, and compared to  
 537 published results in the respective ranges of [NaOH] = 0.1 – 0.3 M, 0.3 – 0.8 M, 0.8 – 1 M, 1 – 5 M.  
 538 This grouping was chosen to constrain the range of NaOH concentrations in the experimental studies  
 539 relatively tightly to the bulk alkali concentrations used in the simulations, while maintaining enough  
 540 data points in each group to enable reliable validation of the thermodynamic model. Results for the  
 541 0.5 M NaOH simulation are shown in Figure 3, and the 0.25 M, 1 M and 3 M NaOH simulations are  
 542 shown in Appendix D.  
 543

544 The maximum Ca content of equilibrated (sodium) calcium silicate hydrate (C-(N-)S-H) gels and the  
545 bulk system alkalinity are inversely related [75]; C-(N-)S-H gels with solid Ca concentrations above  
546 this maximum value are more soluble than portlandite at equilibrium (a maximum value of Ca/Si  $\approx$  1  
547 has been reported for equilibrated C-(N-)S-H gels [75] at bulk NaOH concentrations  $\approx$  1 mol/kg). The  
548 thermodynamic modelling simulations performed here show this same trend (Figure 3 and Appendix  
549 D), which indicate that the C-(N-)S-H gels modelled at a bulk NaOH concentration of 3 M are in  
550 equilibrium with portlandite at all Ca/Si ratios  $\geq$  1, rather than the much higher Ca/Si ratios at which  
551 this is observed in the CaO-SiO<sub>2</sub>-H<sub>2</sub>O system (Ca/Si  $\geq$  1.4, Figure 2).

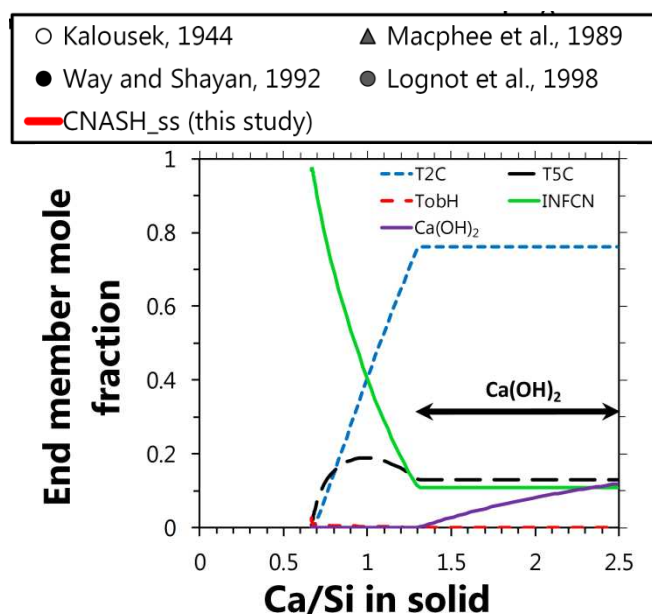
552



553

554

555



556

557 **Figure 3.** Comparison of the simulation results (25°C, 1 bar, 0.5 M NaOH/solids mass ratio = 50) using  
558 the thermodynamic model developed here (CNASH\_ss, bold red traces) to published solubility data  
559 in the CaO-Na<sub>2</sub>O-SiO<sub>2</sub>-H<sub>2</sub>O system at alkali concentrations 0.3 M ≤ [NaOH] ≤ 0.8 M [76, 77, 80, 81].  
560 The simulated C-S-H gels are in equilibrium with portlandite at molar ratios of Ca/Si in the solid ≥ 1.3.  
561 Additional plots are provided in Appendix D for the bulk chemistry results. The thermodynamic  
562 properties of the phases included in these simulations are given in Appendix C.

563

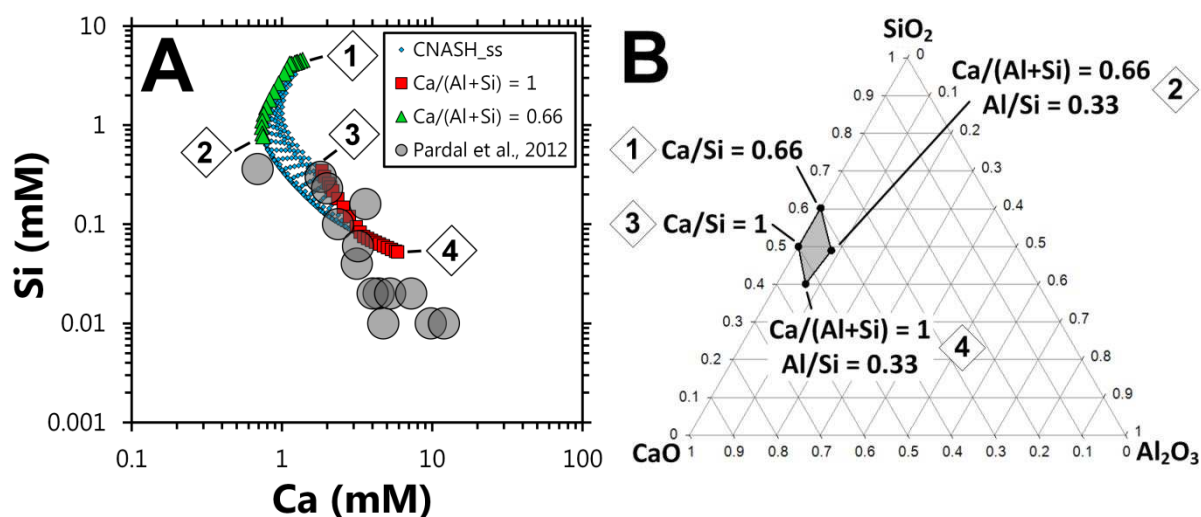
564 The good agreement between the measured solubility data for NaOH concentrations of 0.3 M-0.8 M  
565 and the simulation at [NaOH] = 0.5 M is evident in Figure 3. The composition of the simulated C-(N-  
566 )S-H gel also captures the relatively higher Na content measured in this phase at lower Ca/Si ratios  
567 [77]. The comparisons between the simulated and reported solubility data in the other alkali  
568 concentration ranges studied are also good (Appendix D), with the exception of some of the data  
569 reported at NaOH concentrations > 1 M in [80]. This may be explained by the presence of additional  
570 sodium calcium silicate hydrate gels in those highly alkaline systems that are not described in the  
571 thermodynamic databases used here (e.g. phases with similarities to the kanemite group of minerals  
572 [85], which are thought to be similar to alkali-aggregate reaction products). This would mean that  
573 the aqueous composition data for [NaOH] concentrations > 1 M in [80] may not be solely  
574 determined by the solubility of C-(N-)S-H phases.

575

## 576 6.4 Model validation in the CaO-Al<sub>2</sub>O<sub>3</sub>-SiO<sub>2</sub>-H<sub>2</sub>O system

577 Analysis of C-A-S-H gel solubility from published solubility data for this phase [41, 86] is complicated  
578 by the coexistence of secondary phases such as strätlingite and/or superficial carbonation products  
579 (e.g. calcium hemicarboaluminate, C<sub>4</sub>AC<sub>0.5</sub>H<sub>12</sub>) in the solids analysed. Here, the thermodynamic  
580 model is validated against the solubility dataset published by Pardal et al. [41] (Figure 4) over the  
581 bulk composition range most relevant for AAS cements,  $0.66 \leq \text{Ca}/(\text{Al}+\text{Si}) \leq 1$  and  $0 \leq \text{Al}/\text{Si} \leq 0.33$ .  
582 The simulation results and the measured solubility data are comparable, to within an order of  
583 magnitude. These data show a similar inverse relationship between [Si] and [Ca] to that described by  
584 the solubility data for these elements in the CaO-SiO<sub>2</sub>-H<sub>2</sub>O system (Figure 2).

585



586

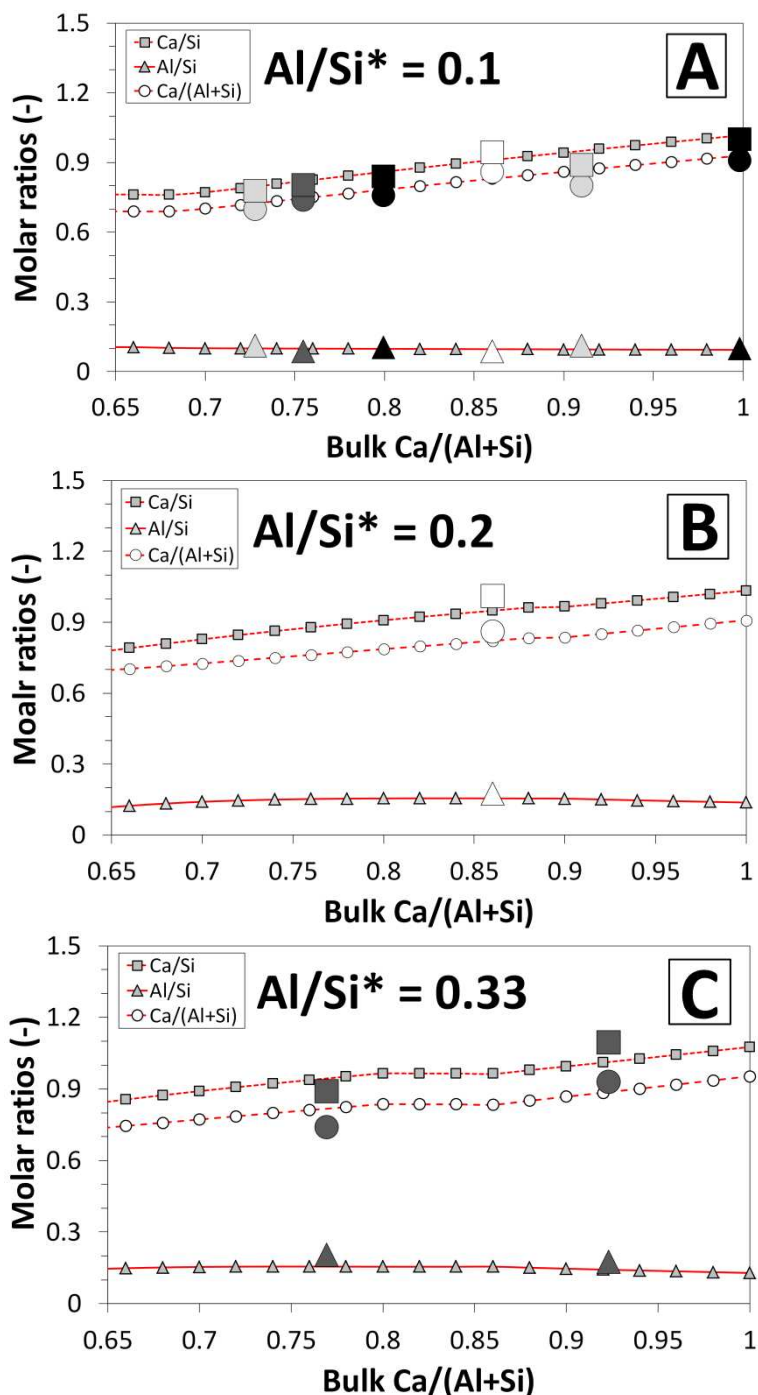
587 **Figure 4.** A) Comparison of the simulation results (25°C, 1 bar, water/solids mass ratio = 50) using the  
588 thermodynamic model developed here (CNASH<sub>ss</sub>, small blue diamonds, red squares and green  
589 triangles) to published solubility data for C-A-S-H gels in the CaO-Al<sub>2</sub>O<sub>3</sub>-SiO<sub>2</sub>-H<sub>2</sub>O system (large grey  
590 circles [41]). The corresponding range of bulk compositions simulated, projected onto the CaO-SiO<sub>2</sub>-  
591 Al<sub>2</sub>O<sub>3</sub> ternary system, is shown in B). The thermodynamic properties of the phases included in these  
592 simulations are given in Appendix C.

593

594 Chemical composition data for C-A-S-H gels are also used for model validation [42, 48, 78, 79]; most  
595 of these data exist at three bulk Al/Si compositions: Al/Si  $\approx$  0.1, 0.2 and 0.33. Comparison of the  
596 modelling results against these data (Figures 5A-5C), for the relevant composition range in AAS

597 binders ( $0.65 \leq \text{bulk Ca}/(\text{Al}+\text{Si}) \leq 1$ ), shows that the simulations accurately describe all of the  
 598 reported chemical composition data for this phase.

599



600

601

602

603 **Figure 5.** Comparison of the simulation results (25°C, 1 bar, water/solids mass ratio = 50) using the  
 604 thermodynamic model developed here (CNASH\_ss, small symbols and red lines) to the published  
 605 chemical composition data for C-A-S-H gels (large symbols represent data from the literature: white  
 606 [42]; light grey [78]; dark grey [48]; black [79]).  $\text{Al}/\text{Si}^* = \text{bulk Al}/\text{Si}$ . Additional plots are provided in

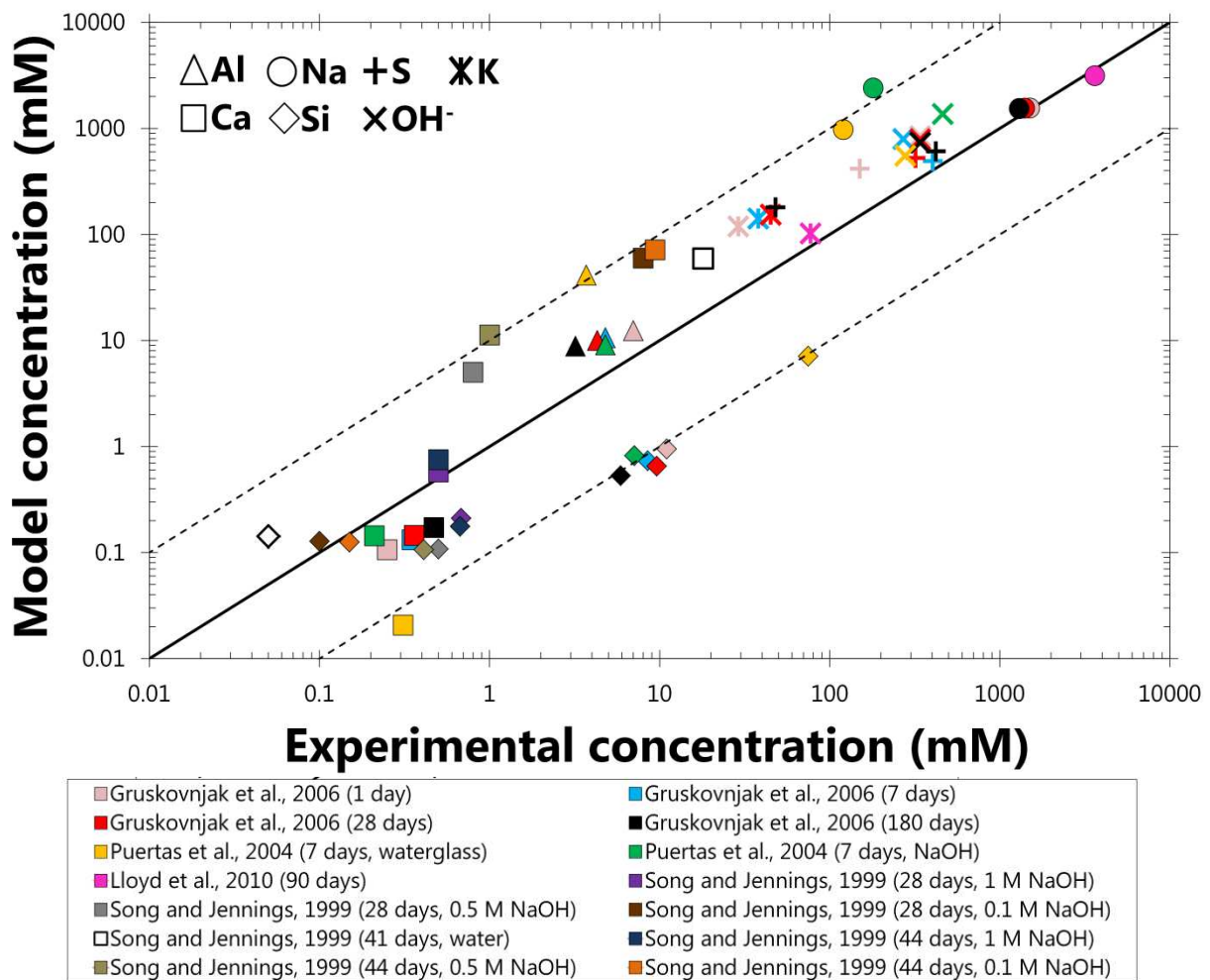
607 Appendix D for the end-member compositions. The thermodynamic properties of the phases  
608 included in these simulations are given in Appendix C.  
609

## 610 **6.5 Model validation in AAS cement systems**

611 Simulations for calculating the solubility of AAS cements were performed in an N<sub>2</sub> atmosphere (1 g of  
612 N<sub>2</sub> (g), to avoid oxidation of the system) at 25°C, 1 bar and at water/binder ratios specified as  
613 reported in the literature (Appendix E). Congruent slag dissolution was assumed, with the slag  
614 reaction extents and bulk chemical compositions simulated by proportional additions of SiO<sub>2</sub>, CaO,  
615 MgO, Al<sub>2</sub>O<sub>3</sub>, Na<sub>2</sub>O, K<sub>2</sub>O, and H<sub>2</sub>SO<sub>4</sub> or dissociated H<sub>2</sub>S<sub>(aq)</sub> (matching the SO<sub>4</sub><sup>2-</sup> and S<sup>2-</sup> content in the  
616 slag where reported, otherwise all sulfur is assumed to be present as S<sup>2-</sup>), to match the bulk slag  
617 chemical compositions and reaction extents reported in the literature (e.g. [45, 87, 88]). All other  
618 components of the slag were excluded, as the concentrations of other elements in the slags studied  
619 are minor and the reactivity of Fe entrained in slag appears to be very low [89]. For the cases where  
620 the degree of reaction of the slag is needed but not available, the extent of reaction of the slag was  
621 set so that the bulk chemistry of the simulations matched the bulk chemistry of the binder gel  
622 assumed in the original work [50], or estimated where no further information was available (using  
623 the reaction extents provided in [87] as reference values, then modifying based on the bulk alkalinity  
624 and curing time).

625  
626 The simulated solubility results (Figure 6) match the experimentally-measured solubility data to  
627 approximately ±1 order of magnitude, with the poorest agreement found for the aqueous Si species  
628 in Na<sub>2</sub>O·*m*SiO<sub>2</sub>·*x*H<sub>2</sub>O-activated cements, which are under-predicted by the thermodynamic model.  
629 However, the uncertainty associated with each experimental data point is expected to be large,  
630 possibly also up to one order of magnitude, because slag reaction extents are not quantified in the  
631 experimental studies referenced here (with the exception of the estimations in [87] for the data in  
632 [71]) and the data correspond to systems that are quite far from equilibrium in some cases (e.g.  
633 samples were cured for 7 days in [82]). Similar slag reaction degrees to those estimated here (~40%

634 at 100 days of curing) have been observed in sodium silicate and NaOH-activated slag pastes (35%-  
 635 45% at 100 days of curing [44]), which does indicate that the estimates used here are reasonable,  
 636 but does not fully resolve the uncertainty attributed to this factor. With this in mind, the accuracy of  
 637 the fit between the simulation and experimental results is similar to the level of uncertainty that can  
 638 be expected for modelling dissolved elemental concentrations in AAS cements.  
 639



640  
 641  
 642 **Figure 6.** Simulated elemental concentrations in the aqueous phase compared to experimental pore  
 643 solution composition data for AAS cements [71, 82-84]. The dotted lines show  $\pm 1$  order of  
 644 magnitude deviation from the solid  $y = x$  line. The thermodynamic properties of the phases included  
 645 in these simulations are given in Appendix C. The slag reaction extents used in these simulations are  
 646 shown in Appendix E.  
 647

648 Comparisons between thermodynamic modelling results and experimental measurements of C-(N-  
 649 )A-S-H gel chemical compositions in AAS cements are not straightforward because secondary

650 products are often intimately intermixed with C-(N-)A-S-H gel in these materials [27] and because  
 651 the nanostructure and chemical composition of this phase can vary considerably at extended ages  
 652 [39]. In this sense, thermodynamic modelling can play an important role in understanding how the  
 653 solid phase assemblage and chemical composition of C-(N-)A-S-H gel may change over time, with  
 654 simulation results representing the predicted nature of the solid binder at equilibrium.

655  
 656 It is also important to assess how accurately the thermodynamic model represents the bulk  
 657 volumetric properties of C-(N-)A-S-H gels, because this is a central aspect of the application of  
 658 thermodynamic modelling to cement-based materials [90]. The C-(N-)A-S-H gels formed in AAS  
 659 cements are significantly denser than the C-S-H gels formed in neat PC materials [50], which is a  
 660 result that should be embodied in thermodynamic models for this phase. Hence simulations using  
 661 the thermodynamic model developed here are compared to the available volumetric data for C-(N-  
 662 )A-S-H gels in AAS cements (Table 3).

663

664 **Table 3.** Simulated C-(N-)A-S-H gel properties in AAS cements [45, 50, 88] compared to the results  
 665 reported in [50], using the bulk chemistry described in that study. The thermodynamic properties of  
 666 the relevant phases in these simulations are given in Appendix C.

Activator	Curing time (days)	Density (g/cm <sup>3</sup> )	Molar volume (cm <sup>3</sup> /mol Si in C-(N-)A-S-H)	Reference
<b>Experimental values</b>				
Na <sub>2</sub> O·1.82SiO <sub>2</sub> ·xH <sub>2</sub> O	90	2.73	50.8	[50]
<b>Simulated values</b>				
Na <sub>2</sub> O·1.82SiO <sub>2</sub> ·xH <sub>2</sub> O	90	2.6	58	[50]
Na <sub>2</sub> SiO <sub>3</sub>	180	2.7	53	COL-GBFS, [88]
Na <sub>2</sub> SiO <sub>3</sub>	180	2.7	54	AUS-GBFS, [88]
Na <sub>2</sub> SiO <sub>3</sub>	180	2.7	53	SP-GBFS, [88]
NaOH	100	2.6	57	[45]
Na <sub>2</sub> SiO <sub>3</sub> ·5H <sub>2</sub> O	100	2.5	56	[45]

667

668 The C-(N-)A-S-H bulk densities and molar volumes simulated by thermodynamic modelling are  
 669 similar to the reported volumetric properties of this phase (Table 3) [50]. This result is consistent  
 670 with a much more tightly packed atomic structure for the C-(N-)A-S-H gels formed in AAS cements

671 than for the C-S-H gels formed in neat PC materials ((CaO)<sub>1.7</sub>(SiO<sub>2</sub>)<sub>1</sub>(H<sub>2</sub>O)<sub>1.8</sub>, molar volume = 72.1  
672 cm<sup>3</sup>/mol [91]). This is also consistent with the discussion presented in [50], where it was argued that  
673 the reported density and molar volume of the C-S-H type gels formed in AAS cements are only  
674 weakly related to the bulk composition of these materials. Therefore, it can be expected that the  
675 thermodynamic model developed here is able to closely represent the bulk volumetric properties of  
676 C-(N-)A-S-H gels in AAS cements.

677

## 678 **6.6 Discussion and perspectives**

679 This paper represents the first step towards developing a structurally-consistent thermodynamic  
680 model for C-(N-)A-S-H gel that contains explicit descriptions of Al and alkali components, which  
681 provides a relatively simple basis for further development and utilisation. Therefore, there are a  
682 number of aspects that would improve the thermodynamic model, and some are listed here to guide  
683 future development:

- 684 • The thermodynamic model has been designed for C-(N-)A-S-H gels with significant Al and  
685 alkali incorporation, particularly those formed in AAS cement. This model may also be  
686 relevant to high volume blended PC/SCM materials reacted with either water or an alkali  
687 source (e.g. CEM III blast furnace cements as specified in EN 197-1), as the bulk chemical  
688 compositions of these materials and AAS cements can be similar ( $\text{Ca}/(\text{Al}+\text{Si}) \approx 1$ ) [92]. Its  
689 suitability for use in simulating the chemistry of these materials needs to be assessed  
690 further.
- 691 • Improvement can be found by removing the assumptions used to simplify the mixing  
692 relationships for the sublattice solid solution model, which approximated the Gibbs free  
693 energies of the reciprocal reactions and the excess Gibbs free energies to zero. This will  
694 become possible as more information is obtained about the energetic differences arising  
695 between hypothetical end-members (i.e. energetic information regarding Si-for-Al

696 substitution in chain sites, and ( $\text{Ca}^{2+}, 2\text{Na}^+, 2\text{H}^+$ ) substitution in interlayer sites) and the  
697 solubility of C-(N-)A-S-H gels.

698 • The utility of the pore solution composition data used to parameterise the thermodynamic  
699 model in AAS cements would be significantly improved if such data were published  
700 alongside quantification of the reaction extent of the slag. This information, along with more  
701 solubility data for AAS cements and synthetic  $\text{CaO-Na}_2\text{O-Al}_2\text{O}_3\text{-SiO}_2\text{-H}_2\text{O}$  systems, will be  
702 needed to enable further development of thermodynamic models for C-(N-)A-S-H gels.

703

704

## 705 **7. Conclusions**

706

707 This paper has presented a thermodynamic model for the C-(N-)A-S-H gel in AAS cements, which for  
708 the first time accounts explicitly for the structurally-incorporated Al and Na species in this phase.  
709 This model represents C-(N-)A-S-H gel as an ideal solid solution of tobermorite-like end-members  
710 with independent substitution of tetrahedral Al and Na species allowed in its formulation, meaning  
711 that it may also be applicable to cement-based materials that are less alkali- and/or Al-rich than AAS  
712 cements. The model was implemented in GEM-Selektor using thermodynamic properties for the C-  
713 (N-)A-S-H end-members that were parameterised to match a comprehensive set of solubility data in  
714 the  $\text{CaO-(Na}_2\text{O,Al}_2\text{O}_3\text{)-SiO}_2\text{-H}_2\text{O}$  and AAS cement systems, and published chemical compositions of C-  
715 A-S-H gels.

716

717 A good fit was found between the full set of data used in the parameterisation procedure and the  
718 simulation results, which were within  $\pm 1$  order of magnitude in simulations of aqueous phase  
719 chemical compositions in AAS cements, indicating that the model is suitable for thermodynamic  
720 modelling of these materials. The molar volume and density of the C-(N-)A-S-H gels simulated by the  
721 model were also in close agreement with the available data for this phase in AAS cements, meaning

722 that the model can describe chemical shrinkage in these systems. Therefore, the thermodynamic  
723 model developed here greatly improves the scope of thermodynamic modelling applications to Ca-  
724 rich alkali-activated cements and hybrid alkali-activated/PC materials, which is important for  
725 understanding the durability of these materials under sealed, ambient and aggressive environmental  
726 conditions.

727

728

## 729 **8. Supporting information**

730

731 The GEM-Selektor database files for the thermodynamic model developed here (CNASH\_ss) are  
732 provided as Electronic Supplementary Information, which can be accessed via the journal website  
733 (<http://www.journals.elsevier.com/cement-and-concrete-research/>).

734

735

## 736 **9. Acknowledgements**

737

738 Special thanks are due to D. A. Kulik, as his contributions on thermodynamic modelling of C-S-H gels  
739 provided the basis for this work [17, 25], to the team behind the freely available GEM-Selektor  
740 thermodynamic modelling program (<http://gems.web.psi.ch/>) [61, 62], and to those involved in the  
741 development of the thermodynamic database for cement related phases (CEMDATA) [17, 23, 64-69].

742 The authors would also like to thank the anonymous reviewers of this paper, whose comments  
743 helped to substantially improve its quality and rigour.

744

745

746        **10.        References**

747

- 748    [1]    H.F.W. Taylor, *Cement Chemistry*, 2<sup>nd</sup> ed., Thomas Telford Publishing, London, 1997.
- 749    [2]    E.P. Flint, L.S. Wells, Study of the system CaO-SiO<sub>2</sub>-H<sub>2</sub>O at 30°C and of the reaction of water  
750        on the anhydrous calcium silicates, *J. Res. Natl. Bur. Stand.*, 12 (1934) 751-783.
- 751    [3]    H.F.W. Taylor, Hydrated calcium silicates. Part I. Compound formation at ordinary  
752        temperatures, *J. Chem. Soc.*, (1950) 3682-3690.
- 753    [4]    K. Fujii, W. Kondo, Heterogeneous equilibrium of calcium silicate hydrate in water at 30°C, *J.*  
754        *Chem. Soc., Dalton Trans.*, (1981) 645-651.
- 755    [5]    A. Atkinson, J.A. Hearne, C.F. Knights, Aqueous chemistry and thermodynamic modelling of  
756        CaO-SiO<sub>2</sub>-H<sub>2</sub>O gels, *J. Chem. Soc., Dalton Trans.*, (1989) 2371-2379.
- 757    [6]    M. Atkins, F.P. Glasser, A. Kindness, Cement hydrate phase: solubility at 25°C, *Cem. Concr.*  
758        *Res.*, 22 (1992) 241-246.
- 759    [7]    F.P. Glasser, M. Tyrer, K. Quillin, D. Ross, J. Pedersen, K. Goldthorpe, D. Bennett, M. Atkins,  
760        The chemistry of blended cements and backfills intended for use in radioactive waste  
761        disposal: R&D technical report P98, Bristol, 1999.
- 762    [8]    J.J. Chen, J.J. Thomas, H.F.W. Taylor, H.M. Jennings, Solubility and structure of calcium  
763        silicate hydrate, *Cem. Concr. Res.*, 34 (2004) 1499-1519.
- 764    [9]    P.S. Roller, G. Ervin, The system calcium oxide-silica-water at 30°C. The association of silicate  
765        ion in dilute alkaline solution, *J. Am. Chem. Soc.*, 62 (1940) 461-471.
- 766    [10]    S.A. Greenberg, T.N. Chang, Investigation of the colloidal hydrated calcium silicates. II.  
767        Solubility relationships in the calcium oxide-silica-water system at 25°C, *J. Phys. Chem.*, 69  
768        (1965) 182-188.
- 769    [11]    K. Suzuki, T. Nishikawa, S. Ito, Formation and carbonation of C-S-H in water, *Cem. Concr.*  
770        *Res.*, 15 (1985) 213-224.
- 771    [12]    M. Grutzeck, A. Benesi, B. Fanning, Silicon-29 magic angle spinning nuclear magnetic  
772        resonance study of calcium silicate hydrates, *J. Am. Ceram. Soc.*, 72 (1989) 665-668.
- 773    [13]    X. Cong, R.J. Kirkpatrick, <sup>29</sup>Si MAS NMR study of the structure of calcium silicate hydrate,  
774        *Adv. Cem. Based Mater.*, 3 (1996) 144-156.
- 775    [14]    A.W. Harris, M.C. Manning, W.M. Tearle, C.J. Tweed, Testing of models of the dissolution of  
776        cements—leaching of synthetic CSH gels, *Cem. Concr. Res.*, 32 (2002) 731-746.
- 777    [15]    C.S. Walker, D. Savage, M. Tyrer, K.V. Ragnarsdottir, Non-ideal solid solution aqueous  
778        solution modeling of synthetic calcium silicate hydrate, *Cem. Concr. Res.*, 37 (2007) 502-511.
- 779    [16]    H.M. Jennings, Aqueous solubility relationships for two types of calcium silicate hydrate, *J.*  
780        *Am. Ceram. Soc.*, 69 (1986) 614-618.

- 781 [17] D.A. Kulik, M. Kersten, Aqueous solubility diagrams for cementitious waste stabilization  
782 systems: II. End-member stoichiometries of ideal calcium silicate hydrate solid solutions, J.  
783 Am. Ceram. Soc., 84 (2001) 3017-3026.
- 784 [18] U.R. Berner, Evolution of pore water chemistry during degradation of cement in a  
785 radioactive waste repository environment, Waste Manage., 12 (1992) 201-219.
- 786 [19] F.P. Glasser, E.E. Lachowski, D.E. Macphee, Compositional model for calcium silicate hydrate  
787 (C-S-H) gels, their solubilities, and free energies of formation, J. Am. Ceram. Soc., 70 (1987)  
788 481-485.
- 789 [20] E.J. Reardon, An ion interaction model for the determination of chemical equilibria in  
790 cement/water systems, Cem. Concr. Res., 20 (1990) 175-192.
- 791 [21] M. Atkins, D.G. Bennett, A.C. Dawes, F.P. Glasser, A. Kindness, D. Read, A thermodynamic  
792 model for blended cements, Cem. Concr. Res., 22 (1992) 497-502.
- 793 [22] J.A. Gisby, R.H. Davies, A.T. Dinsdale, M. Tyrer, F.P. Glasser, J. Hill, P. Livesey, C. Walker, C-S-  
794 H solubility modeling at different temperatures, in: Proceedings of the 12th International  
795 Congress on the Chemistry of Cement, Cement Association of Canada, Montreal, 2007.
- 796 [23] B. Lothenbach, F. Winnefeld, Thermodynamic modelling of the hydration of Portland  
797 cement, Cem. Concr. Res., 36 (2006) 209-226.
- 798 [24] B. Lothenbach, Thermodynamic equilibrium calculations in cementitious systems, Mater.  
799 Struct., 43 (2010) 1413-1433.
- 800 [25] D.A. Kulik, Improving the structural consistency of C-S-H solid solution thermodynamic  
801 models, Cem. Concr. Res., 41 (2011) 477-495.
- 802 [26] B. Lothenbach, K. Scrivener, R.D. Hooton, Supplementary cementitious materials, Cem.  
803 Concr. Res., 41 (2011) 1244-1256.
- 804 [27] I.G. Richardson, G.W. Groves, Microstructure and microanalysis of hardened cement pastes  
805 involving ground granulated blast-furnace slag, J. Mater. Sci., 27 (1992) 6204-6212.
- 806 [28] J.L. Provis, S.A. Bernal, Geopolymers and related alkali-activated materials, Annu. Rev.  
807 Mater. Res., 44 (2014) 3.1-3.29.
- 808 [29] C. Shi, P.V. Krivenko, D. Roy, Alkali-Activated Cements and Concretes, 1<sup>st</sup> ed., Taylor &  
809 Francis, New York, 2006.
- 810 [30] M. Atkins, F. Glasser, L.P. Moroni, J.J. Jack, Thermodynamic modelling of blended cements at  
811 elevated temperature (50-90°C), Aberdeen University, United Kingdom,  
812 DoE1HMIP1RR/94.011, 1994.
- 813 [31] M. Ben Haha, B. Lothenbach, G. Le Saoût, F. Winnefeld, Influence of slag chemistry on the  
814 hydration of alkali-activated blast-furnace slag - part II: effect of Al<sub>2</sub>O<sub>3</sub>, Cem. Concr. Res., 42  
815 (2012) 74-83.
- 816 [32] W. Loewenstein, The distribution of aluminum in the tetrahedra of silicates and aluminates,  
817 Am. Mineral., 39 (1954) 92-96.

- 818 [33] L. Pegado, C. Labbez, S.V. Churakov, Mechanism of aluminium incorporation into C-S-H from  
819 ab initio calculations, *J. Mater. Chem. A*, 2 (2014) 3477-3483.
- 820 [34] I.G. Richardson, A.R. Brough, R. Brydson, G.W. Groves, C.M. Dobson, Location of aluminum  
821 in substituted calcium silicate hydrate (C-S-H) gels as determined by  $^{29}\text{Si}$  and  $^{27}\text{Al}$  NMR and  
822 EELS, *J. Am. Ceram. Soc.*, 76 (1993) 2285-2288.
- 823 [35] I.G. Richardson, A.R. Brough, G.W. Groves, C.M. Dobson, The characterization of hardened  
824 alkali-activated blast-furnace slag pastes and the nature of the calcium silicate hydrate (C-S-  
825 H) phase, *Cem. Concr. Res.*, 24 (1994) 813-829.
- 826 [36] F. Puertas, M. Palacios, H. Manzano, J.S. Dolado, A. Rico, J. Rodríguez, A model for the C-A-S-  
827 H gel formed in alkali-activated slag cements, *J. Eur. Ceram. Soc.*, 31 (2011) 2043-2056.
- 828 [37] F. Bonk, J. Schneider, M.A. Cincotto, H. Panepucci, Characterization by multinuclear high-  
829 resolution NMR of hydration products in activated blast-furnace slag pastes, *J. Am. Ceram.*  
830 *Soc.*, 86 (2003) 1712-1719.
- 831 [38] I.G. Richardson, G.W. Groves, The incorporation of minor and trace elements into calcium  
832 silicate hydrate (C-S-H) gel in hardened cement pastes, *Cem. Concr. Res.*, 23 (1993) 131-138.
- 833 [39] R.J. Myers, S.A. Bernal, R. San Nicolas, J.L. Provis, Generalized structural description of  
834 calcium-sodium aluminosilicate hydrate gels: the cross-linked substituted tobermorite  
835 model, *Langmuir*, 29 (2013) 5294-5306.
- 836 [40] A. Fernández-Jiménez, F. Puertas, I. Sobrados, J. Sanz, Structure of calcium silicate hydrates  
837 formed in alkaline-activated slag: Influence of the type of alkaline activator, *J. Am. Ceram.*  
838 *Soc.*, 86 (2003) 1389-1394.
- 839 [41] X. Pardal, F. Brunet, T. Charpentier, I. Pochard, A. Nonat,  $^{27}\text{Al}$  and  $^{29}\text{Si}$  solid-state NMR  
840 characterization of calcium-aluminosilicate-hydrate, *Inorg. Chem.*, 51 (2012) 1827-1836.
- 841 [42] G.K. Sun, J.F. Young, R.J. Kirkpatrick, The role of Al in C-S-H: NMR, XRD, and compositional  
842 results for precipitated samples, *Cem. Concr. Res.*, 36 (2006) 18-29.
- 843 [43] S.D. Wang, K.L. Scrivener, Hydration products of alkali activated slag cement, *Cem. Concr.*  
844 *Res.*, 25 (1995) 561-571.
- 845 [44] M. Ben Haha, G. Le Saoût, F. Winnefeld, B. Lothenbach, Influence of activator type on  
846 hydration kinetics, hydrate assemblage and microstructural development of alkali activated  
847 blast-furnace slags, *Cem. Concr. Res.*, 41 (2011) 301-310.
- 848 [45] G. Le Saoût, M. Ben Haha, F. Winnefeld, B. Lothenbach, Hydration degree of alkali-activated  
849 slags: a  $^{29}\text{Si}$  NMR study, *J. Am. Ceram. Soc.*, 94 (2011) 4541-4547.
- 850 [46] A.R. Brough, A. Atkinson, Sodium silicate-based, alkali-activated slag mortars - Part I.  
851 Strength, hydration and microstructure, *Cem. Concr. Res.*, 32 (2002) 865-879.
- 852 [47] X. Pardal, I. Pochard, A. Nonat, Experimental study of Si-Al substitution in calcium-silicate-  
853 hydrate (C-S-H) prepared under equilibrium conditions, *Cem. Concr. Res.*, 39 (2009) 637-643.

- 854 [48] P. Faucon, A. Delagrave, J.C. Petit, C. Richet, J.M. Marchand, H. Zanni, Aluminum  
855 incorporation in calcium silicate hydrates (C-S-H) depending on their Ca/Si ratio, *J. Phys.*  
856 *Chem. B*, 103 (1999) 7796-7802.
- 857 [49] H.M. Jennings, Refinements to colloid model of C-S-H in cement: CM-II, *Cem. Concr. Res.*, 38  
858 (2008) 275-289.
- 859 [50] J.J. Thomas, A.J. Allen, H.M. Jennings, Density and water content of nanoscale solid C-S-H  
860 formed in alkali-activated slag (AAS) paste and implications for chemical shrinkage, *Cem.*  
861 *Concr. Res.*, 42 (2012) 377-383.
- 862 [51] E. Bonaccorsi, S. Merlino, A.R. Kampf, The crystal structure of tobermorite 14Å (plombierite),  
863 a C-S-H phase, *J. Am. Ceram. Soc.*, 88 (2005) 505-512.
- 864 [52] S. Merlino, E. Bonaccorsi, T. Armbruster, The real structure of tobermorite 11Å: normal and  
865 anomalous forms, OD character and polytypic modifications, *Eur. J. Mineral.*, 13 (2001) 577-  
866 590.
- 867 [53] I.G. Richardson, Tobermorite/jennite- and tobermorite/calcium hydroxide-based models for  
868 the structure of C-S-H: applicability to hardened pastes of tricalcium silicate,  $\beta$ -dicalcium  
869 silicate, Portland cement, and blends of Portland cement with blast-furnace slag,  
870 metakaolin, or silica fume, *Cem. Concr. Res.*, 34 (2004) 1733-1777.
- 871 [54] I.G. Richardson, The calcium silicate hydrates, *Cem. Concr. Res.*, 38 (2008) 137-158.
- 872 [55] I.G. Richardson, G.W. Groves, Models for the composition and structure of calcium silicate  
873 hydrate (CSH) gel in hardened tricalcium silicate pastes, *Cem. Concr. Res.*, 22 (1992) 1001-  
874 1010.
- 875 [56] A.J. Allen, J.J. Thomas, H.M. Jennings, Composition and density of nanoscale calcium-silicate-  
876 hydrate in cement, *Nat. Mater.*, 6 (2007) 311-316.
- 877 [57] M. Hillert, Phase equilibria, phase diagrams and phase transformations: their  
878 thermodynamic basis, Cambridge University Press, Cambridge, 1998.
- 879 [58] M. Hillert, L.-I. Staffansson, The regular solution model for stoichiometric phases and ionic  
880 melts, *Acta Chem. Scand.*, 24 (1970) 3618-3626.
- 881 [59] J.O. Andersson, A.F. Guillermet, M. Hillert, B. Jansson, B. Sundman, A compound-energy  
882 model of ordering in a phase with sites of different coordination numbers, *Acta Metall.*  
883 *Mater.*, 34 (1986) 437-445.
- 884 [60] J.L. Provis, P. Duxson, G.C. Lukey, J.S.J. Van Deventer, Statistical thermodynamic model for  
885 Si/Al ordering in amorphous aluminosilicates, *Chem. Mater.*, 17 (2005) 2976-2986.
- 886 [61] D.A. Kulik, T. Wagner, S.V. Dmytrieva, G. Kosakowski, F.F. Hingerl, K.V. Chudnenko, U.  
887 Berner, GEM-Selektor geochemical modeling package: revised algorithm and GEMS3K  
888 numerical kernel for coupled simulation codes, *Comput. Geosci.*, 17 (2013) 1-24.
- 889 [62] T. Wagner, D.A. Kulik, F.F. Hingerl, S.V. Dmytrieva, GEM-Selektor geochemical modeling  
890 package: TSolMod library and data interface for multicomponent phase models, *Can.*  
891 *Mineral.*, 50 (2012) 1173-1195.

- 892 [63] W. Hummel, U. Berner, E. Curti, F.J. Pearson, T. Thoenen, Nagra/PSI Chemical  
893 Thermodynamic Database 01/01, Universal Publishers, Parkland, 2002.
- 894 [64] T. Matschei, B. Lothenbach, F.P. Glasser, Thermodynamic properties of Portland cement  
895 hydrates in the system CaO-Al<sub>2</sub>O<sub>3</sub>-SiO<sub>2</sub>-CaSO<sub>4</sub>-CaCO<sub>3</sub>-H<sub>2</sub>O, *Cem. Concr. Res.*, 37 (2007) 1379-  
896 1410.
- 897 [65] T. Schmidt, B. Lothenbach, M. Romer, K. Scrivener, D. Rentsch, R. Figi, A thermodynamic and  
898 experimental study of the conditions of thaumasite formation, *Cem. Concr. Res.*, 38 (2008)  
899 337-349.
- 900 [66] B. Lothenbach, T. Matschei, G. Möschner, F.P. Glasser, Thermodynamic modelling of the  
901 effect of temperature on the hydration and porosity of Portland cement, *Cem. Concr. Res.*,  
902 38 (2008) 1-18.
- 903 [67] D.A. Kulik, M. Kersten, Aqueous solubility diagrams for cementitious waste stabilization  
904 systems. 4. A carbonation model for Zn-doped calcium silicate hydrate by Gibbs energy  
905 minimization, *Environ. Sci. Technol.*, 36 (2002) 2926-2931.
- 906 [68] G. Möschner, B. Lothenbach, J. Rose, A. Ulrich, R. Figi, R. Kretzschmar, Solubility of Fe-  
907 ettringite (Ca<sub>6</sub>[Fe(OH)<sub>6</sub>]<sub>2</sub>(SO<sub>4</sub>)<sub>3</sub>·26H<sub>2</sub>O), *Geochim. Cosmochim. Acta*, 72 (2008) 1-18.
- 908 [69] G. Möschner, B. Lothenbach, F. Winnefeld, A. Ulrich, R. Figi, R. Kretzschmar, Solid solution  
909 between Al-ettringite and Fe-ettringite (Ca<sub>6</sub>[Al<sub>1-x</sub>Fe<sub>x</sub>(OH)<sub>6</sub>]<sub>2</sub>(SO<sub>4</sub>)<sub>3</sub>·26H<sub>2</sub>O), *Cem. Concr. Res.*,  
910 39 (2009) 482-489.
- 911 [70] H.C. Helgeson, D.H. Kirkham, G.C. Flowers, Theoretical prediction of the thermodynamic  
912 behavior of aqueous electrolytes at high pressures and temperatures: IV. Calculation of  
913 activity coefficients, osmotic coefficients, and apparent molal and standard and relative  
914 partial molal properties to 600°C and 5 kb, *Am. J. Sci.*, 281 (1981) 1249-1516.
- 915 [71] A. Gruskovnjak, B. Lothenbach, L. Holzer, R. Figi, F. Winnefeld, Hydration of alkali-activated  
916 slag: Comparison with ordinary Portland cement, *Adv. Cem. Res.*, 18 (2006) 119-128.
- 917 [72] K.S. Pitzer, Ion interaction approach: theory and data correlation, in: *Activity Coefficients in*  
918 *Electrolyte Solutions*, CRC Press, Boca Raton, 1991, 75-153.
- 919 [73] J.L. Provis, P. Duxson, G.C. Lukey, F. Separovic, W.M. Kriven, J.S.J. Van Deventer, Modeling  
920 speciation in highly concentrated alkaline silicate solutions, *Ind. Eng. Chem. Res.*, 44 (2005)  
921 8899-8908.
- 922 [74] G.M. Anderson, D.A. Crerar, *Thermodynamics in geochemistry: the equilibrium model*,  
923 Oxford University Press, Oxford, 1993.
- 924 [75] I. Lognot, I. Klur, A. Nonat, NMR and infrared spectroscopies of C-S-H and Al-substituted C-S-  
925 H synthesised in alkaline solutions, in: P. Colombet, H. Zanni, A.-R. Grimmer, P. Sozzani (Eds.)  
926 *Nuclear magnetic resonance spectroscopy of cement-based materials*, Springer Berlin  
927 Heidelberg, 1998, 189-196.
- 928 [76] S.Y. Hong, F.P. Glasser, Alkali binding in cement pastes: part I. The C-S-H phase, *Cem. Concr.*  
929 *Res.*, 29 (1999) 1893-1903.

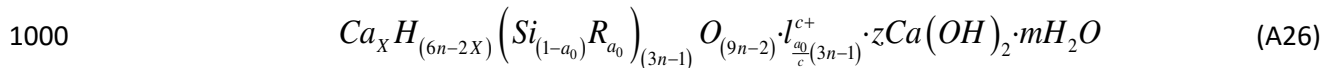
- 930 [77] S.J. Way, A. Shayan, Study of some synthetically prepared hydrous alkali calcium silicates,  
931 *Cem. Concr. Res.*, 22 (1992) 915-926.
- 932 [78] G. Renaudin, J. Russias, F. Leroux, F. Frizon, C. Cau-dit-Coumes, Structural characterization of  
933 C-S-H and C-A-S-H samples - part I: long-range order investigated by Rietveld analyses, *J.*  
934 *Solid State Chem.*, 182 (2009) 3312-3319.
- 935 [79] G. Renaudin, J. Russias, F. Leroux, C. Cau-dit-Coumes, F. Frizon, Structural characterization of  
936 C-S-H and C-A-S-H samples - part II: local environment investigated by spectroscopic  
937 analyses, *J. Solid State Chem.*, 182 (2009) 3320-3329.
- 938 [80] G.L. Kalousek, Studies of portions of the quaternary system soda-lime-silica-water at 25°C, *J.*  
939 *Res. Natl. Bur. Stand.*, 32 (1944) 285-302.
- 940 [81] D.E. Macphee, K. Luke, F.P. Glasser, E.E. Lachowski, Solubility and aging of calcium silicate  
941 hydrates in alkaline solutions at 25°C, *J. Am. Ceram. Soc.*, 72 (1989) 646-654.
- 942 [82] F. Puertas, A. Fernández-Jiménez, M.T. Blanco-Varela, Pore solution in alkali-activated slag  
943 cement pastes. Relation to the composition and structure of calcium silicate hydrate, *Cem.*  
944 *Concr. Res.*, 34 (2004) 139-148.
- 945 [83] R.R. Lloyd, J.L. Provis, J.S.J. van Deventer, Pore solution composition and alkali diffusion in  
946 inorganic polymer cement, *Cem. Concr. Res.*, 40 (2010) 1386-1392.
- 947 [84] S. Song, H.M. Jennings, Pore solution chemistry of alkali-activated ground granulated blast-  
948 furnace slag, *Cem. Concr. Res.*, 29 (1999) 159-170.
- 949 [85] R.J. Kirkpatrick, A.G. Kalinichev, X. Hou, L. Struble, Experimental and molecular dynamics  
950 modeling studies of interlayer swelling: water incorporation in kanemite and ASR gel, *Mater.*  
951 *Struct.*, 38 (2005) 449-458.
- 952 [86] P. Faucon, J.C. Petit, T. Charpentier, J.F. Jacquinet, F. Adenot, Silicon Substitution for  
953 Aluminum in Calcium Silicate Hydrates, *J. Am. Ceram. Soc.*, 82 (1999) 1307-1312.
- 954 [87] B. Lothenbach, A. Gruskovnjak, Hydration of alkali-activated slag: thermodynamic modelling,  
955 *Adv. Cem. Res.*, 19 (2007) 81-92.
- 956 [88] S.A. Bernal, R. San Nicolas, R.J. Myers, R. Mejía de Gutiérrez, F. Puertas, J.S.J. van Deventer,  
957 J.L. Provis, MgO content of slag controls phase evolution and structural changes induced by  
958 accelerated carbonation in alkali-activated binders, *Cem. Concr. Res.*, 57 (2014) 33-43.
- 959 [89] S.A. Bernal, V. Rose, J.L. Provis, The fate of iron in blast furnace slag particles during alkali-  
960 activation, *Mater. Chem. Phys.*, 146 (2014) 1-5.
- 961 [90] B. Lothenbach, G. Le Saout, E. Gallucci, K. Scrivener, Influence of limestone on the hydration  
962 of Portland cements, *Cem. Concr. Res.*, 38 (2008) 848-860.
- 963 [91] A.J. Allen, J.J. Thomas, Analysis of C-S-H gel and cement paste by small-angle neutron  
964 scattering, *Cem. Concr. Res.*, 37 (2007) 319-324.
- 965 [92] R. Taylor, I.G. Richardson, R.M.D. Brydson, Composition and microstructure of 20-year-old  
966 ordinary Portland cement-ground granulated blast-furnace slag blends containing 0 to 100%  
967 slag, *Cem. Concr. Res.*, 40 (2010) 971-983.

- 968 [93] R.A. Robie, B.S. Hemingway, Thermodynamic properties of minerals and related substances  
969 at 298.15 K and 1 bar ( $10^5$  Pascals) pressure and at higher temperatures, United States  
970 Government Printing Office, Washington D.C., 1995.
- 971 [94] H.C. Helgeson, J.M. Delany, H.W. Nesbitt, Summary and critique of the thermodynamic  
972 properties of rock-forming minerals, *Am. J. Sci.*, 278-A (1978).
- 973 [95] M.W. Chase, Jr., NIST-JANAF Thermochemical Tables, Fourth Edition, *J. Phys. Chem. Ref.*  
974 *Data*, 4<sup>th</sup> Ed., 1998.
- 975 [96] D.D. Wagman, W.H. Evans, V.B. Parker, R.H. Schumm, I. Halow, The NBS tables of chemical  
976 thermodynamic properties: selected values for inorganic and  $C_1$  and  $C_2$  organic substances in  
977 SI units, American Chemical Society and the American Institute of Physics for the National  
978 Bureau of Standards, New York, 1982.
- 979 [97] E.L. Shock, D.C. Sassani, M. Willis, D.A. Sverjensky, Inorganic species in geologic fluids:  
980 correlations among standard molal thermodynamic properties of aqueous ions and  
981 hydroxide complexes, *Geochim. Cosmochim. Acta*, 61 (1997) 907-950.
- 982 [98] D.A. Sverjensky, E.L. Shock, H.C. Helgeson, Prediction of the thermodynamic properties of  
983 aqueous metal complexes to 1000°C and 5 kb, *Geochim. Cosmochim. Acta*, 61 (1997) 1359-  
984 1412.
- 985 [99] E.L. Shock, H.C. Helgeson, D.A. Sverjensky, Calculation of the thermodynamic and transport  
986 properties of aqueous species at high pressures and temperatures: standard partial molal  
987 properties of inorganic neutral species, *Geochim. Cosmochim. Acta*, 53 (1989) 2157-2183.
- 988 [100] J.W. Johnson, E.H. Oelkers, H.C. Helgeson, SUPCRT92: A software package for calculating the  
989 standard molal thermodynamic properties of minerals, gases, aqueous species, and  
990 reactions from 1 to 5000 bar and 0 to 1000°C, *Comput. Geosci.*, 18 (1992) 899-947.
- 991 [101] B. Lothenbach, L. Pelletier-Chaignat, F. Winnefeld, Stability in the system  $CaO-Al_2O_3-H_2O$ ,  
992 *Cem. Concr. Res.*, 42 (2012) 1621-1634.
- 993
- 994

995 **Appendix A. Additional details of the C-(N-)A-S-H sublattice solid**  
 996 **solution model**

997

998 Derivation of the C-(N-)A-S-H thermodynamic model begins by rearranging the SGM (eq.(A1), [38])  
 999 into an alternative structural form:

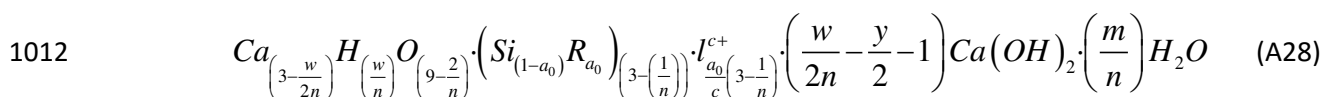


1001 where  $R$  is a trivalent cation in tetrahedral coordination (e.g.  $Al^{3+}$ ),  $l$  is a charge-balancing interlayer  
 1002 cation (such as  $Ca^{2+}$ ) with a positive charge of  $c$ ,  $m$  defines the amount of bound interlayer water,  $n$  is  
 1003 the number of dreierketten units per non-crosslinked C-(N-)A-S-H chain,  $a_0$  is the extent of  
 1004 substitution in aluminosilicate chains and the parameters  $X$ ,  $z$ ,  $a_0$  and  $n$  are defined according to  
 1005 eq.(A2):

1006 
$$\left. \begin{aligned} X &= 0.5(6n - w) \\ z &= 0.5[w + n(y - 2)] \\ 0 \leq a_0 &\leq \frac{n-1}{(3n-1)} \end{aligned} \right\} \quad (A27)$$

1007

1008 The parameters  $w$  and  $y$  are related to the extent of protonation of chain tetrahedra and amount of  
 1009 solid solution  $Ca(OH)_2$  present in the gel. Rearrangement of the SGM begins by normalising eq.(A1)  
 1010 to a basis of one dreierketten unit by dividing by  $n$ , expressed in terms of  $w$  and  $n$  for  $X$  and  $z$ , and  
 1011 then simplified to obtain eq.(A3):



1013

1014 The following notation is now introduced into eq.(A3):  $v = 1/n$  ( $0 \leq v \leq 1$ ), defines the ratio of chains  
 1015 per dreierketten unit, which is a measure of the number of vacant bridging tetrahedra;  $u = w/n$ , the

1016 content of chemically incorporated (hydroxyl) water per dreierketten unit; and  $h = m/n$ , the bound  
 1017 water content. The introduction of this notation results in eq.(A4):

$$1018 \quad Ca_{\left(3-\frac{u}{2}\right)} H_u O_{(9-2v)} \cdot \left( Si_{(1-a)} R_{a_0} \right)_{(3-v)} \cdot I_{\frac{a_0}{c}(3-v)}^{c+} \cdot \left( \frac{u}{2} - \frac{y}{2} - 1 \right) Ca(OH)_2 \cdot hH_2O \quad (A29)$$

1019

1020 Eq.(A4) is then re-written to isolate two distinct sublattice sites within the chain structure, being a  
 1021 ‘main chain dreierketten unit’ (*TU*) and a ‘bridging tetrahedral unit’ (*BT*). This leads to a subtle  
 1022 change in the substitution parameter,  $a_0$ , which is now written as  $a$ , the extent of substitution in  
 1023 bridging sites. The resulting equation is:

$$1024 \quad \left[ Ca(OH)_2 \right]_{\left(\frac{u+y-2}{2}\right)} \cdot \left[ (CaSiO_{3.5})_2 \right] \cdot \left[ \left( Si_{(1-a)} R_a O_2 \right)_{(1-v)} \right]^{a(1-v)-} \cdot \left[ \left( I_{\frac{a}{c}(1-v)}^{c+} \right) \right]^{a(1-v)+} \cdot \left[ Ca_{\left(1-\frac{u}{2}\right)} H_u \right]^{2+} \cdot hH_2O \quad (A30)$$

1025

1026 Eq.(A5) is equivalent to eq.(2) in the main body of the text.

1027

1028 **Appendix B. Activity coefficient relationships for the C-(N-)A-S-H end-**  
 1029 **members**

1030

1031 The relationships for the fictive activity coefficients for the end-members of the C-(N-)A-S-H  
 1032 sublattice solid solution model are defined here in terms of the following notation: 5CA = 0, INFCA =  
 1033 1, 5CNA = 2, INFCNA = 3, INFCN = 4, T2C\* = 5, T5C\* = 6, TobH\* = 7.

1034

1035 
$$\ln(\lambda_0) = 2\ln(\chi_0 + \chi_1) + 2\ln(\chi_0 + \chi_1) + 2\ln(\chi_0 + \chi_2 + \chi_5 + \chi_6) +$$
  

$$\ln(\chi_0 + \chi_5 + \chi_6) + \ln(\chi_0 + \chi_5 + \chi_6) + \ln(\chi_0 + \chi_1 + \chi_2 + \chi_3 + \chi_4) - \ln(\chi_0) \quad (\text{B31})$$

1036 
$$\ln(\lambda_1) = 2\ln(\chi_0 + \chi_1) + 2\ln(\chi_0 + \chi_1) + 2\ln(\chi_1 + \chi_4 + \chi_7) +$$
  

$$\ln(\chi_1) + \ln(\chi_1 + \chi_4 + \chi_7) + \ln(\chi_0 + \chi_1 + \chi_2 + \chi_3 + \chi_4) - \ln(\chi_1) \quad (\text{B32})$$

1037 
$$\ln(\lambda_2) = 2\ln(\chi_2 + \chi_3) + 2\ln(\chi_2 + \chi_3) + 2\ln(\chi_0 + \chi_2 + \chi_5 + \chi_6) +$$
  

$$\ln(\chi_2) + \ln(\chi_2) + \ln(\chi_0 + \chi_1 + \chi_2 + \chi_3 + \chi_4) - \ln(\chi_2) \quad (\text{B33})$$

1038 
$$\ln(\lambda_3) = 2\ln(\chi_2 + \chi_3) + 2\ln(\chi_2 + \chi_3) + 2\ln(\chi_3) +$$
  

$$\ln(\chi_3) + \ln(\chi_3) + \ln(\chi_0 + \chi_1 + \chi_2 + \chi_3 + \chi_4) - \ln(\chi_3) \quad (\text{B34})$$

1039 
$$\ln(\lambda_4) = 2\ln(\chi_4) + 2\ln(\chi_4) + 2\ln(\chi_1 + \chi_4 + \chi_7) +$$
  

$$\ln(\chi_4) + \ln(\chi_1 + \chi_4 + \chi_7) + \ln(\chi_0 + \chi_1 + \chi_2 + \chi_3 + \chi_4) - \ln(\chi_4) \quad (\text{B35})$$

1040 
$$\ln(\lambda_5) = 2\ln(\chi_5) + 2\ln(\chi_5) + 2\ln(\chi_0 + \chi_2 + \chi_5 + \chi_6) +$$
  

$$\ln(\chi_0 + \chi_5 + \chi_6) + \ln(\chi_0 + \chi_5 + \chi_6) + \ln(\chi_5 + \chi_6 + \chi_7) - \ln(\chi_5) \quad (\text{B36})$$

1041 
$$\ln(\lambda_6) = 2\ln(\chi_6 + \chi_7) + 2\ln(\chi_6 + \chi_7) + 2\ln(\chi_0 + \chi_2 + \chi_5 + \chi_6) +$$
  

$$\ln(\chi_0 + \chi_5 + \chi_6) + \ln(\chi_0 + \chi_5 + \chi_6) + \ln(\chi_5 + \chi_6 + \chi_7) - \ln(\chi_6) \quad (\text{B37})$$

1042 
$$\ln(\lambda_7) = 2\ln(\chi_6 + \chi_7) + 2\ln(\chi_6 + \chi_7) + 2\ln(\chi_1 + \chi_4 + \chi_7) +$$
  

$$\ln(\chi_7) + \ln(\chi_1 + \chi_4 + \chi_7) + \ln(\chi_5 + \chi_6 + \chi_7) - \ln(\chi_7) \quad (\text{B38})$$

1043

1044 **Appendix C. Thermodynamic properties of the constituent phases and**  
 1045 **the relevant phases for thermodynamic modelling in this work**

1046

1047 The solid constituents used in the additivity method and eq.(23), to estimate the standard absolute  
 1048 isobaric heat capacity and absolute entropy at standard state of the C-(N-)A-S-H end-members, are  
 1049 shown in Table C1. The gases, aqueous species and solid phases used in the thermodynamic  
 1050 modelling simulations are shown in Tables C2-C4.

1051

1052 Table C1. Thermodynamic properties of the solid constituents used to estimate  $Cp^\circ$  and  $S^\circ$  for the C-  
 1053 (N-)A-S-H end-members. The reference state is 298.15 K and 1 bar.

Phase	$V^\circ$ (cm <sup>3</sup> /mol)	$\Delta_f H^\circ$ (kJ/mol)	$\Delta_f G^\circ$ (kJ/mol)	$S^\circ$ (J/mol.K)	$Cp^\circ$ (J/mol.K)	Reference
Portlandite, Ca(OH) <sub>2</sub>	33.1	-984.7	-897.0	83.4	87.5	[93]
Amorphous SiO <sub>2</sub>	29.0	-903.3	-848.9	41.3	44.5	[17, 94]
Gibbsite, Al(OH) <sub>3</sub>	32.0	-1289	-1151	70.1	93.1	[94]
NaOH <sub>(s)</sub>	18.8	-425.8	-379.6	64.4	59.5	[93, 95]
T2C, (CaO) <sub>1.5</sub> (SiO <sub>2</sub> ) <sub>1</sub> (H <sub>2</sub> O) <sub>2.5</sub>	80.6	-2722	-2467	167	237	[25]

1054

1055

1056 **Table C2.** Thermodynamic properties of the gases used in the thermodynamic modelling simulations.  
 1057 The reference state is 298.15 K and 1 bar.

Gas	$V^\circ$ (cm <sup>3</sup> /mol)	$\Delta_f H^\circ$ (kJ/mol)	$\Delta_f G^\circ$ (kJ/mol.K)	$S^\circ$ (J/mol.K)	$Cp^\circ$ (J/mol.K)	Reference
N <sub>2</sub>	24790	0	0	191.6	29.1	[96]
O <sub>2</sub>	24790	0	0	205.1	29.3	[96]
H <sub>2</sub>	24790	0	0	130.7	28.8	[96]

1058

1059

1060

1061

1062

1063

1064

1065 **Table C3.** Thermodynamic properties of the aqueous species used in the thermodynamic modelling  
 1066 simulations. The reference state is unit activity in a hypothetical one molal solution referenced to  
 1067 infinite dilution at any temperature and pressure for aqueous species [70].

Species	$V^\circ$ (cm <sup>3</sup> /mol)	$\Delta_f H^\circ$ (kJ/mol)	$\Delta_f G^\circ$ (kJ/mol.K)	$S^\circ$ (J/mol.K)	$C_p^\circ$ (J/mol.K)	Reference
Al <sup>3+</sup>	-45.2	-530.6	-483.7	-325.1	-128.7	[97]
AlO <sup>+</sup> (+ H <sub>2</sub> O = Al(OH) <sub>2</sub> <sup>+</sup> )	0.3	-713.6	-660.4	-113	-125.1	[97]
AlO <sub>2</sub> <sup>-</sup> (+ 2H <sub>2</sub> O = Al(OH) <sub>4</sub> <sup>-</sup> )	9.5	-925.6	-827.5	-30.2	-49	[97]
AlOOH <sup>0</sup> (+ 2H <sub>2</sub> O = Al(OH) <sub>3</sub> <sup>0</sup> )	13	-947.1	-864.3	20.9	-209.2	[97]
AlOH <sup>2+</sup>	-2.7	-767.3	-692.6	-184.9	56	[97]
AlHSiO <sub>3</sub> <sup>2+</sup> (+ H <sub>2</sub> O = AlSiO(OH) <sub>3</sub> <sup>2+</sup> )	-40.7	-1718	-1541	-304.2	-215.9	[64]
AlSiO <sub>4</sub> <sup>-</sup> (+ 3H <sub>2</sub> O = AlSiO(OH) <sub>6</sub> <sup>-</sup> )	25.5	-1834	-1681	11.1	-4.6	[64]
AlSO <sub>4</sub> <sup>+</sup>	-6.0	-1423	-1250	-172.4	-204.0	[64]
Al(SO <sub>4</sub> ) <sub>2</sub> <sup>-</sup>	31.1	-2338	-2006	-135.5	-268.4	[64]
Ca <sup>2+</sup>	-18.4	-543.1	-552.8	-56.5	-30.9	[97]
CaOH <sup>+</sup>	5.8	-751.6	-717	28	6	[97]
Ca(HSiO <sub>3</sub> ) <sup>+</sup> (+ H <sub>2</sub> O = CaSiO(OH) <sub>3</sub> <sup>+</sup> )	-6.7	-1687	-1574	-8.3	137.8	[98]
CaSiO <sub>3</sub> <sup>0</sup> (+ H <sub>2</sub> O = CaSiO <sub>2</sub> (OH) <sub>2</sub> <sup>0</sup> )	15.7	-1668	-1518	-136.7	88.9	[64]
CaSO <sub>4</sub> <sup>0</sup>	4.7	-1448	-1310	20.9	-104.6	[98]
K <sup>+</sup>	9.0	-252.1	-282.5	101	8.4	[97]
KOH <sup>0</sup>	15	-474.1	-437.1	108.4	-85	[97]
KSO <sub>4</sub> <sup>-</sup>	27.5	-1159	-1032	146.4	-45.1	[98]
Na <sup>+</sup>	-1.2	-240.3	-261.9	58.4	38.1	[97]
NaOH <sup>0</sup>	3.5	-470.1	-418.1	44.8	-13.4	[97]
NaSO <sub>4</sub> <sup>-</sup>	18.6	-1147	-1010	101.8	-30.1	[64]
HSiO <sub>3</sub> <sup>-</sup> (+ H <sub>2</sub> O = SiO(OH) <sub>3</sub> <sup>-</sup> )	4.5	-1145	-1014	20.9	-87.2	[98]
SiO <sub>2</sub> <sup>0</sup>	16.1	-887.9	-833.4	41.3	44.5	[17, 99]
SiO <sub>3</sub> <sup>2-</sup> (+ H <sub>2</sub> O = SiO <sub>2</sub> (OH) <sub>2</sub> <sup>2-</sup> )	34.1	-1099	-938.5	-80.2	119.8	[64]
S <sub>2</sub> O <sub>3</sub> <sup>2-</sup>	27.6	-649.9	-520.0	66.9	-238.5	[97]
HSO <sub>3</sub> <sup>-</sup>	33.0	-627.7	-529.1	139.7	-5.4	[97]
SO <sub>3</sub> <sup>2-</sup>	-4.1	-636.9	-487.9	-29.3	-281.0	[97]
HSO <sub>4</sub> <sup>-</sup>	34.8	-889.2	-755.8	125.5	22.7	[97]
SO <sub>4</sub> <sup>2-</sup>	12.9	-909.7	-744.5	18.8	-266.1	[97]
H <sub>2</sub> S <sup>0</sup>	35.0	-39.0	-27.9	125.5	179.2	[99]
HS <sup>-</sup>	20.2	-16.2	12.0	68.2	-93.9	[97]
S <sup>2-</sup>	20.2	92.2	120.4	68.2	-93.9	[63]
Mg <sup>2+</sup>	-22.0	-465.9	-454.0	-138.1	-21.7	[97]
MgOH <sup>+</sup>	1.6	-690.0	-625.9	-79.9	129.2	[97]
MgHSiO <sub>3</sub> <sup>+</sup> (+ H <sub>2</sub> O = MgSiO(OH) <sub>3</sub> <sup>+</sup> )	-10.9	-1614	-1477	-99.5	158.6	[97]
MgSO <sub>4</sub> <sup>0</sup>	1.8	-1369	-1212	-50.9	-90.3	[63, 97]
MgSiO <sub>3</sub> <sup>0</sup> (+ H <sub>2</sub> O = MgSiO <sub>2</sub> (OH) <sub>2</sub> <sup>0</sup> )	12.1	-1597	-1425	-218.3	98.2	[63]
OH <sup>-</sup>	-4.7	-230	-157.3	-10.7	-136.3	[97]
H <sup>+</sup>	0	0	0	0	0	[97]
H <sub>2</sub> O <sup>0</sup>	18.1	-285.9	-237.2	69.9	75.4	[100]
N <sub>2</sub> <sup>0</sup>	33.4	-10.4	18.2	95.8	234.2	[99]
O <sub>2</sub> <sup>0</sup>	30.5	-12.2	16.4	109	234.1	[99]

1068

1069

1070

1071

1072 **Table C4.** Thermodynamic properties of the solid phases used in the thermodynamic modelling  
1073 simulations. The reference state is 298.15 K and 1 bar.

Phase	$V^\circ$ (cm <sup>3</sup> /mol)	$\Delta_f H^\circ$ (kJ/mol)	$\Delta_f G^\circ$ (kJ/mol.K)	$S^\circ$ (J/mol.K)	$C_p^\circ$ (J/mol.K)	Reference
Al(OH) <sub>3</sub> (microcrystalline)	32.0	-1265	-1148	140	93.1	[101]
Portlandite, Ca(OH) <sub>2</sub>	33.1	-984.7	-897	83.4	87.5	[93]
Amorphous SiO <sub>2</sub>	29.0	-903.3	-849	41.3	44.5	[17, 94]
C <sub>2</sub> AH <sub>8</sub>	90.1	-5278	-4696	450	521	[101]
C <sub>3</sub> AH <sub>6</sub>	150	-5537	-5008	422	446	[101]
C <sub>4</sub> AH <sub>13</sub>	27.4	-8302	-7327	700	930	[66]
C <sub>4</sub> AH <sub>19</sub>	382	-1002	-8750	1120	1382	[101]
C <sub>4</sub> AH <sub>10</sub>	194	-5388	-4623	610	668	[101]
Monosulfate, C <sub>4</sub> AsH <sub>12</sub>	309	-8750	-7779	821	942	[64]
Stratlingite, C <sub>2</sub> ASH <sub>8</sub>	21.6	-6360	-5705	546	603	[64]
Ettringite, C <sub>6</sub> As <sub>3</sub> H <sub>32</sub>	707	-17535	-15206	1900	2174	[66]
Hydrotalcite, M <sub>4</sub> AH <sub>10</sub>	220	-7196	-6395	549	649	[66]
Brucite, Mg(OH) <sub>2</sub>	24.6	-923	-832	63.1	77.3	[94]
<b>The 'downscaled CSH3T' model <sup>a</sup></b>						
TobH, (CaO) <sub>1</sub> (SiO <sub>2</sub> ) <sub>1.5</sub> (H <sub>2</sub> O) <sub>2.5</sub>	85.0	-2833	-2562	153	231	[25]
T5C, (CaO) <sub>1.25</sub> (SiO <sub>2</sub> ) <sub>1.25</sub> (H <sub>2</sub> O) <sub>2.5</sub>	79.3	-2782	-2519	160	234	[25]
T2C, (CaO) <sub>1.5</sub> (SiO <sub>2</sub> ) <sub>1</sub> (H <sub>2</sub> O) <sub>2.5</sub>	80.6	-2722	-2467	167	237	[25]

1074 <sup>a</sup> The mixing rules used to describe the downscaled CSH3T model and the thermodynamic properties  
1075 that define the TobH, T5C and T2C end-members in GEM-Selektor are the same as those described  
1076 in [25] for this model. The Gibbs free energies (and thus the enthalpies) of these components are  
1077 modified slightly to the corresponding values used to define the TobH\*, T5C\* and T2C\* end-  
1078 members of the CNASH\_ss model (Table 2).

1079

1080

1081

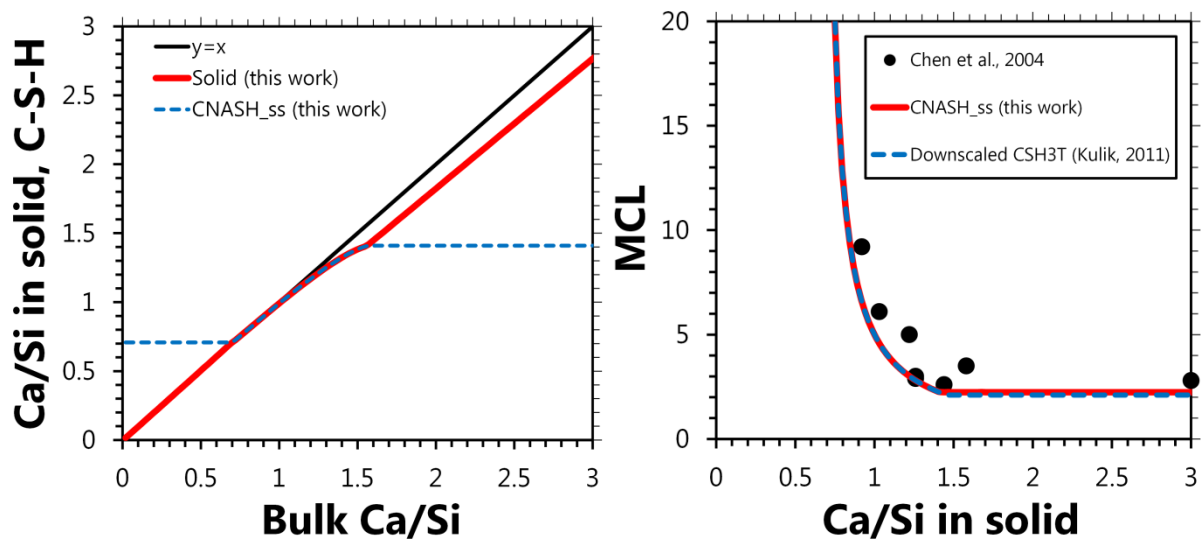
1082 **Appendix D. Additional simulation results used to validate the**  
1083 **thermodynamic model**

1084

1085 Additional simulation results that were used to validate the thermodynamic model are shown in

1086 Figures D1-D6.

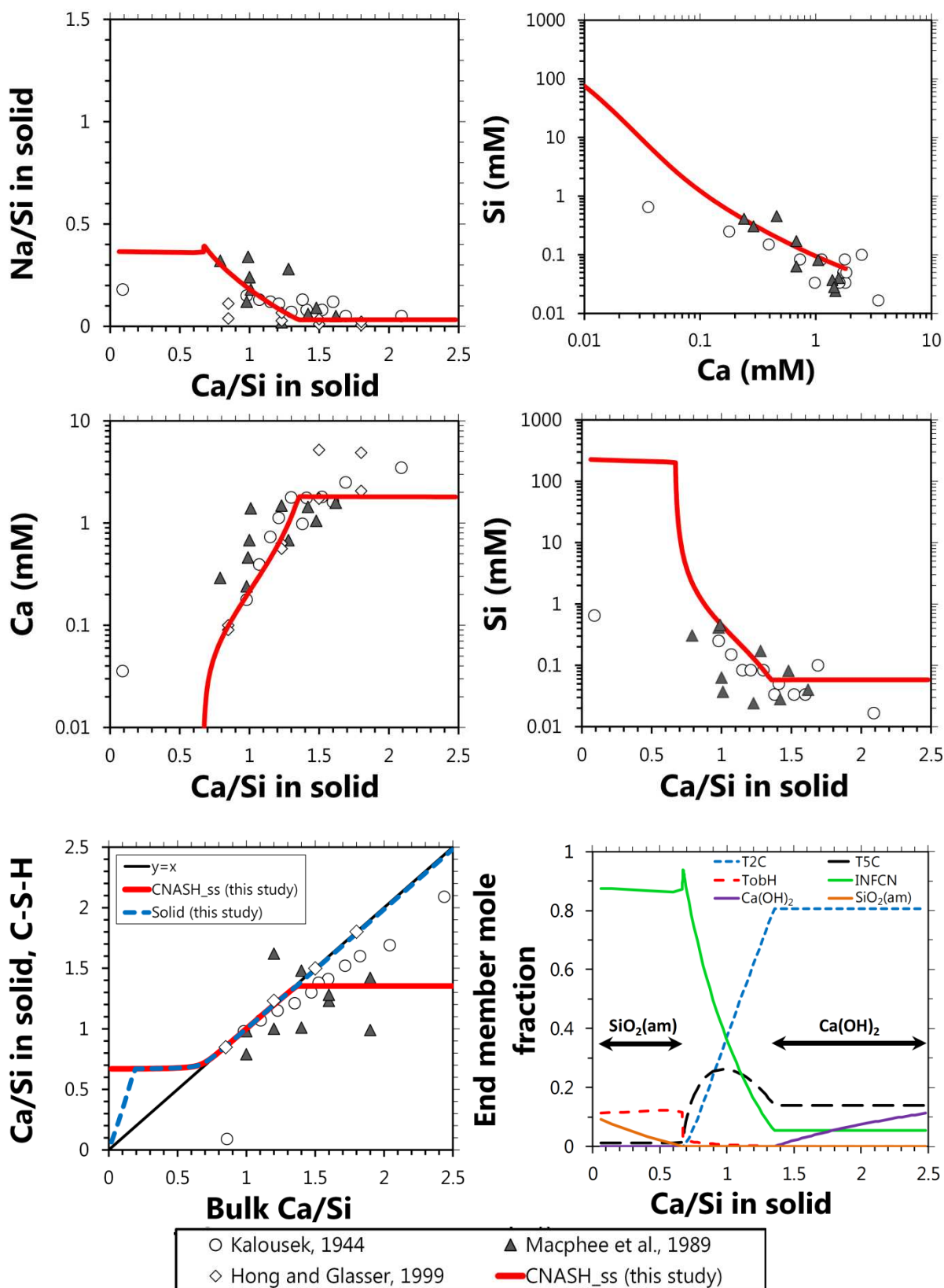
1087



1088

1089 **Figure D1.** Simulation results (25°C, 1 bar, 0.25 M NaOH/solids mass ratio = 50) using the  
1090 thermodynamic model developed here (CNASH\_ss) in addition to those presented in Figure 2. The  
1091 MCL calculations are compared to the data reported in [8] and the simulation results using the  
1092 downscaled CSH3T model [25]. The thermodynamic properties of the phases included in these  
1093 simulations are given in Appendix C.

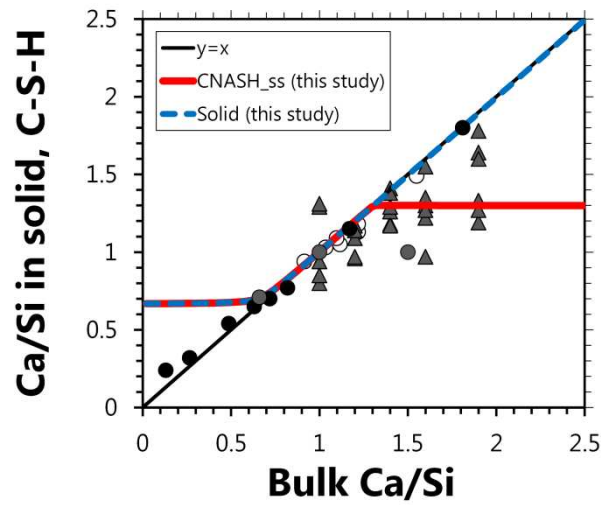
1094



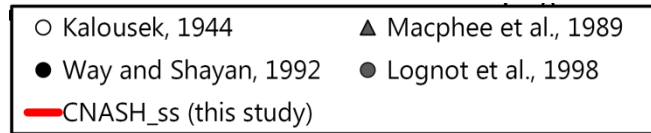
1099 **Figure D2.** Comparison of the simulation results (25°C, 1 bar, 0.25 M NaOH/solids mass ratio = 50)  
 1100 using the thermodynamic model developed here (CNASH\_ss, bold red traces) to published solubility  
 1101 data in the CaO-Na<sub>2</sub>O-SiO<sub>2</sub>-H<sub>2</sub>O system at alkali concentrations 0.1 M ≤ [NaOH] ≤ 0.3 M [76, 80, 81].  
 1102 The thermodynamic properties of the phases included in these simulations are given in Appendix C.

1103

1104



1105

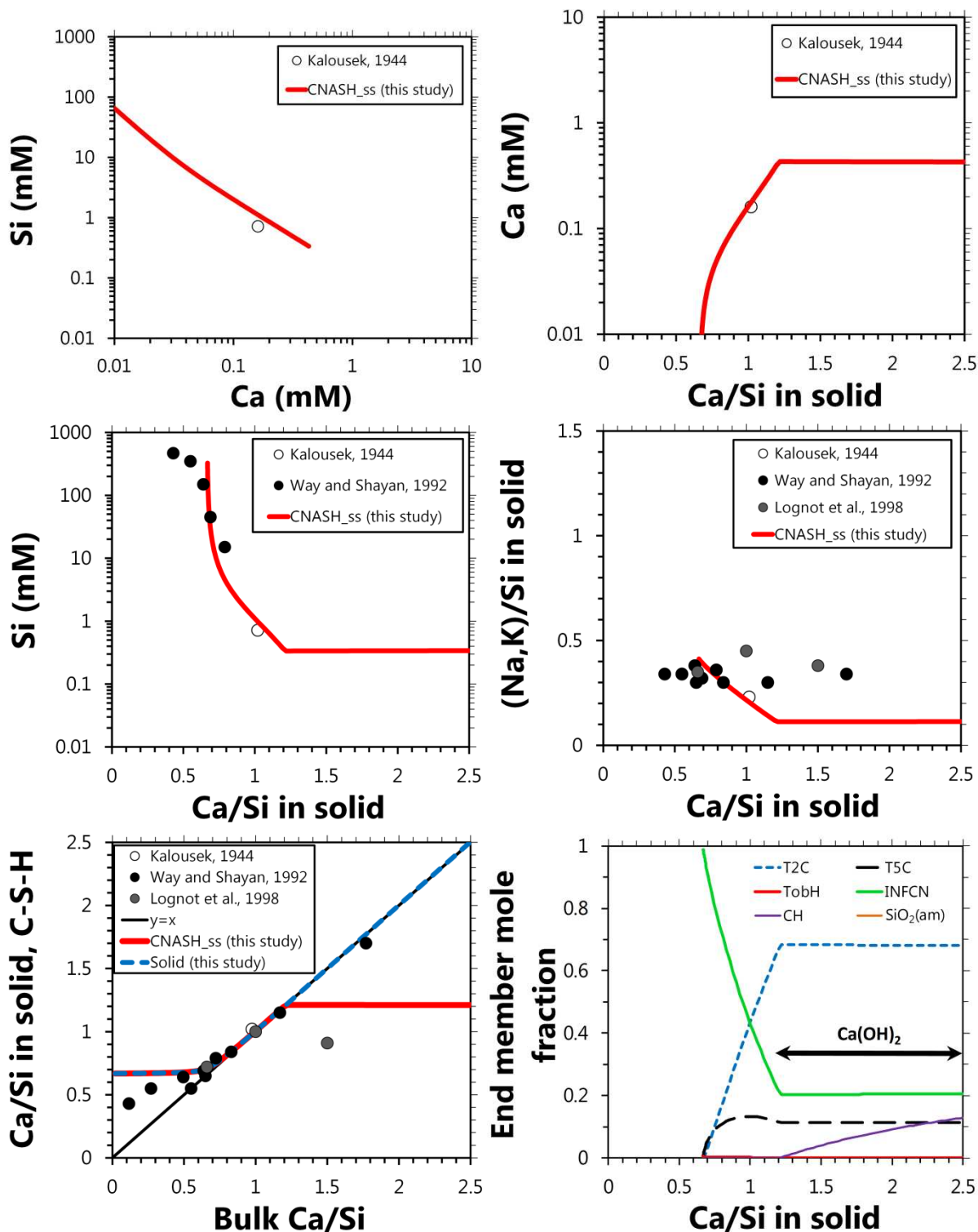


1106

1107 **Figure D3.** Comparison of the simulation results (25°C, 1 bar, 0.5 M NaOH/solids mass ratio = 50)  
1108 using the thermodynamic model developed here (CNASH\_ss, bold red traces) to solid chemistry data  
1109 in the CaO-Na<sub>2</sub>O-SiO<sub>2</sub>-H<sub>2</sub>O system at alkali concentrations 0.3 M ≤ [NaOH] ≤ 0.8 M [76, 80, 81], in  
1110 addition to the results shown in Figure 3 for this system. The thermodynamic properties of the  
1111 phases included in these simulations are given in Appendix C.

1112

1113



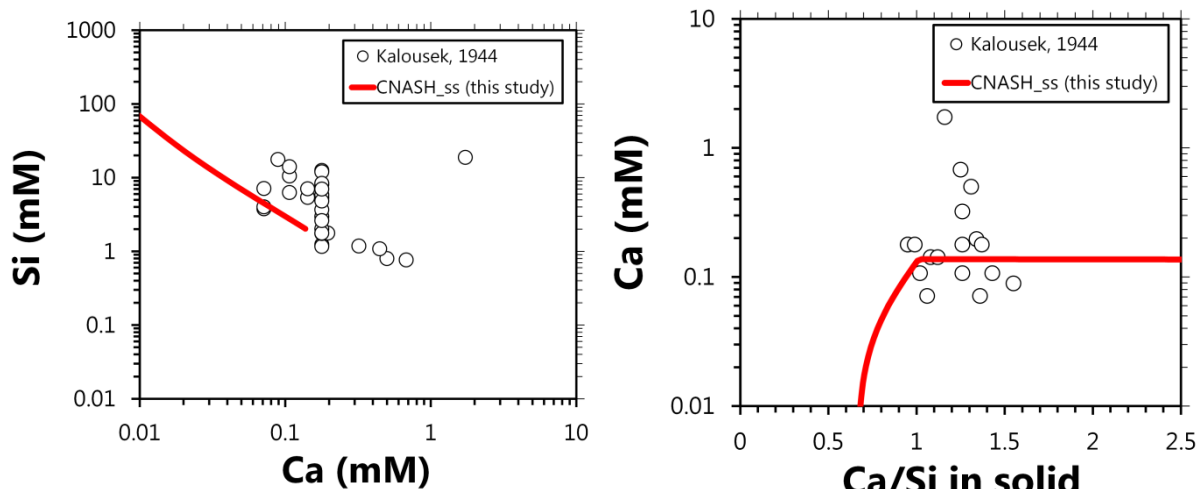
1114

1115

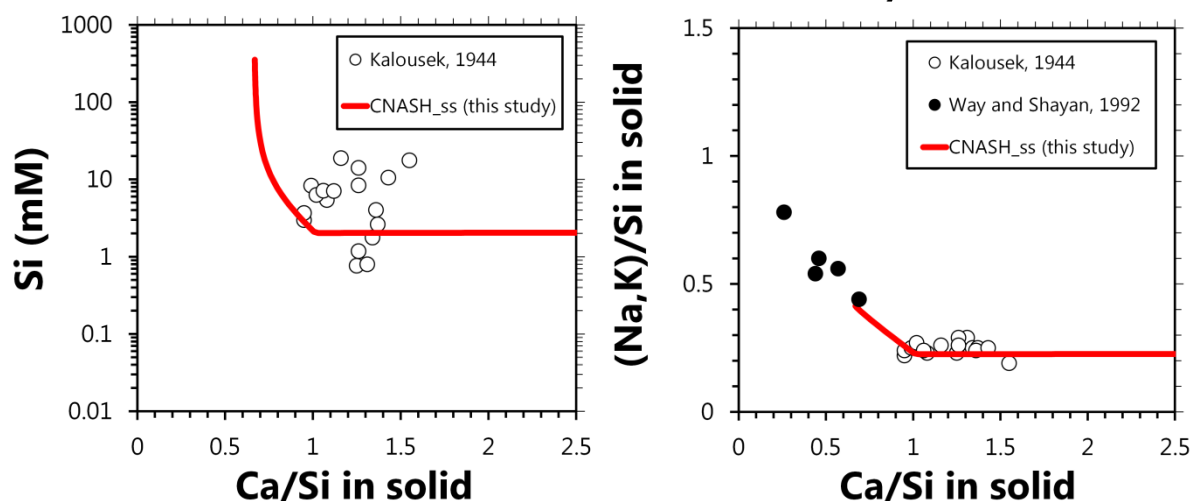
1116

1117 **Figure D4.** Comparison of the simulation results (25°C, 1 bar, 1 M NaOH/solids mass ratio = 50) using  
 1118 the thermodynamic model developed here (CNASH<sub>ss</sub>, bold red traces) to solubility and solid phase  
 1119 chemistry data in the CaO-Na<sub>2</sub>O-SiO<sub>2</sub>-H<sub>2</sub>O system at alkali concentrations 0.8 M ≤ [NaOH] ≤ 1 M [75,  
 1120 77, 80]. The corresponding end member mole fraction results are also shown. The thermodynamic  
 1121 properties of the phases included in these simulations are given in Appendix C.  
 1122

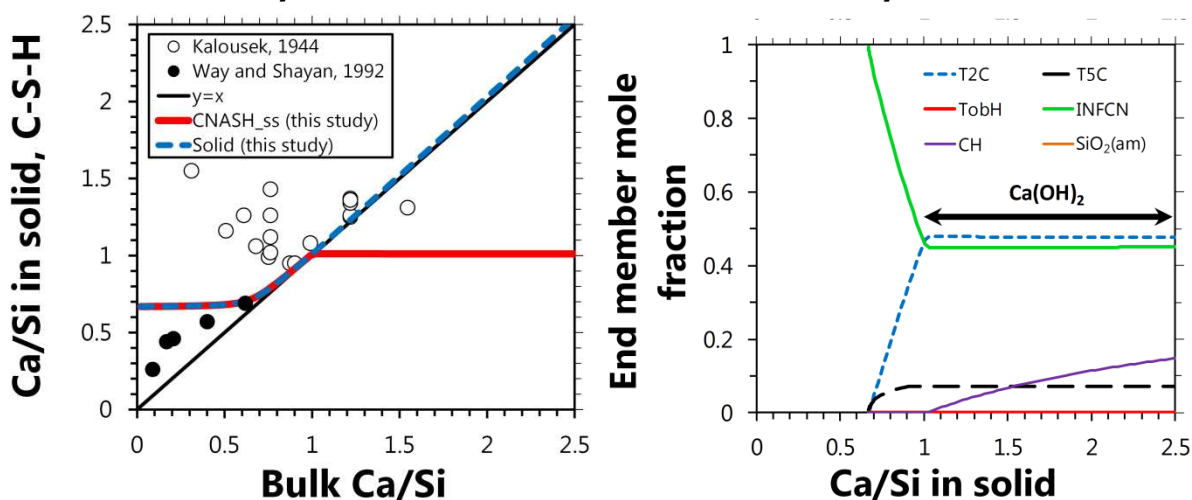
1123



1124



1125

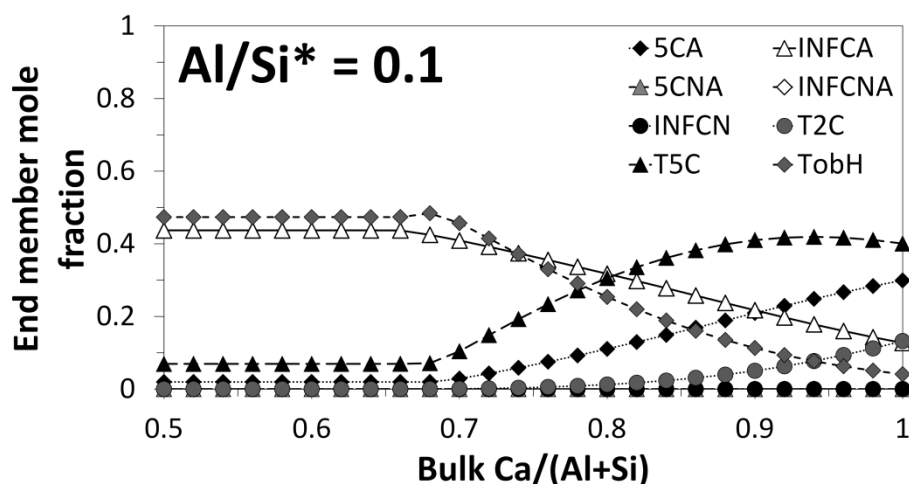


1126

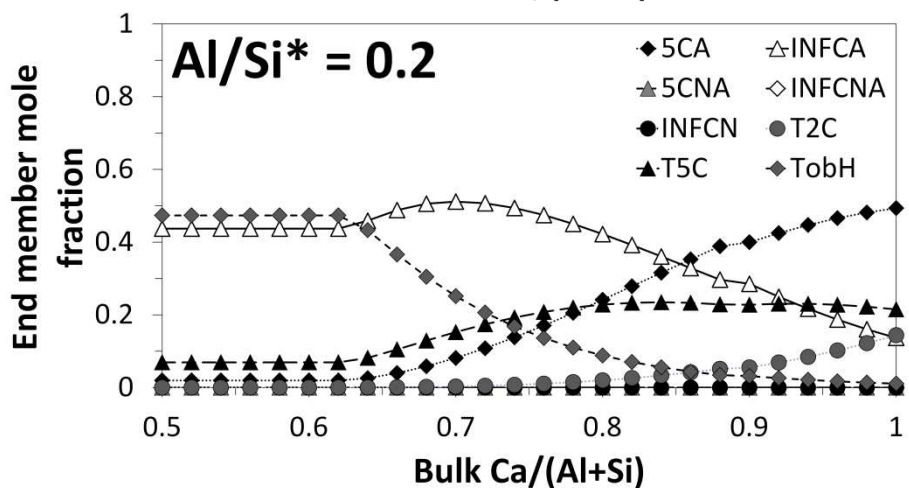
1127 **Figure D5.** Comparison of the simulation results (25°C, 1 bar, 3 M NaOH/solids mass ratio = 50) using  
 1128 the thermodynamic model developed here (CNASH<sub>ss</sub>, bold red traces) to solubility and solid phase  
 1129 chemistry data in the CaO-Na<sub>2</sub>O-SiO<sub>2</sub>-H<sub>2</sub>O system at alkali concentrations 1 M ≤ [NaOH] ≤ 5 M [77,  
 1130 80]. The corresponding end member mole fraction results are also shown. The thermodynamic  
 1131 properties of the phases included in these simulations are given in Appendix C.

1132

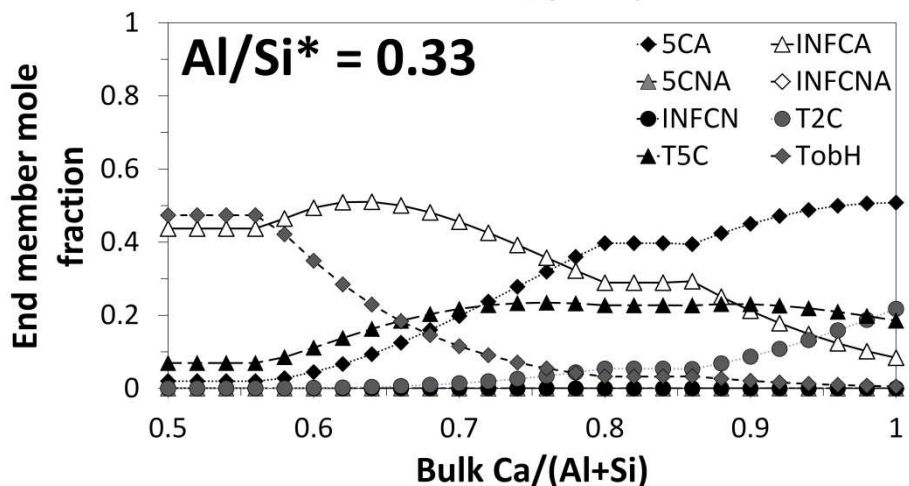
1133



1134



1135



1136

1137 **Figure D6.** End member mole fractions corresponding to the simulation results shown in Figure 5  
1138 (25°C, 1 bar, water/solids mass ratio = 50). Al/Si\* = bulk Al/Si. The thermodynamic properties of the  
1139 phases included in these simulations are given in Appendix C.

1140

1141 **Appendix E. Additional details of the AAS cements simulated by**  
 1142 **thermodynamic modelling**

1143

1144 The slag reaction extents, curing times and activating conditions used to simulate the pore solution  
 1145 chemistry of AAS cements (Figure 6) are shown in Table E1.

1146

1147 **Table E1.** Slag reaction extents, curing times and activating conditions used to simulate the pore  
 1148 solution chemistry of AAS cements.

System (corresponding to the legend labels in Figure 6)	Curing time (days)	Activator	Water/binder	Slag reaction extent used in simulations (%)	Reference
Gruskovnjak et al., 2006	1	Na <sub>2</sub> SiO <sub>3</sub> ·5H <sub>2</sub> O	0.3 <sup>a</sup>	32	[71]
Gruskovnjak et al., 2006	7	Na <sub>2</sub> SiO <sub>3</sub> ·5H <sub>2</sub> O	0.3 <sup>a</sup>	36	[71, 87]
Gruskovnjak et al., 2006	28	Na <sub>2</sub> SiO <sub>3</sub> ·5H <sub>2</sub> O	0.3 <sup>a</sup>	38	[71, 87]
Gruskovnjak et al., 2006	180	Na <sub>2</sub> SiO <sub>3</sub> ·5H <sub>2</sub> O	0.3 <sup>a</sup>	42	[71, 87]
Puertas et al., 2004	7	Na <sub>2</sub> O·1.5SiO <sub>2</sub> ·xH <sub>2</sub> O	0.5 <sup>b</sup>	36	[82]
Puertas et al., 2004	7	NaOH	0.5 <sup>b</sup>	36	[82]
Lloyd et al., 2010	90	Na <sub>2</sub> O·mSiO <sub>2</sub> ·xH <sub>2</sub> O	0.35	40	[83]
Song and Jennings, 1999	28	1 M NaOH	0.45 <sup>c</sup>	36	[84]
Song and Jennings, 1999	28	0.5 M NaOH	0.45 <sup>c</sup>	31	[84]
Song and Jennings, 1999	28	0.1 M NaOH	0.45 <sup>c</sup>	26	[84]
Song and Jennings, 1999	41	H <sub>2</sub> O	0.45 <sup>c</sup>	21	[84]
Song and Jennings, 1999	44	1 M NaOH	0.45 <sup>c</sup>	39	[84]
Song and Jennings, 1999	44	0.5 M NaOH	0.45 <sup>c</sup>	34	[84]
Song and Jennings, 1999	44	0.1 M NaOH	0.45 <sup>c</sup>	29	[84]

1149 <sup>a</sup> water/cement.

1150 <sup>b</sup> (water + activator)/slag.

1151 <sup>c</sup> liquid/slag.

1152

1153

1154